Inverse Modeling to Verify California's Greenhouse Gas Emission Inventory

Report Version 1.2

Contract Number 09-348

Investigators:

Marc L. Fischer and Seongeun Jeong
California State University East-Bay
and Lawrence Berkeley National Laboratory

June, 2012

Prepared for the
California Air Resources Board and
the California Environmental Protection Agency

DISCLAIMER

The statements and conclusions in this Report are those of the contractor and not necessarily those of the California Air Resources Board. The mention of commercial products, their source, or their use in the connection with material reported herein is not to be construed as actual or implied endorsement of such products.

ACKNOWLEDGEMENT

This report was submitted in fulfillment of California Air Resources Board (CARB) Contract number 09-348. We thank Arlyn E. Andrews, Laura Bianco, James M. Wilczak, Dave Field, Dave Bush, Edward Wahl, Fabien Guerin, Yuchen Yi, and particularly Jon Kofler for assistance with measurements at WGC and analysis of data from radar wind profiler sites, John Lin, Christoph Gerbig, Steve Wofsy, Janusz Eluszkiewicz, Thomas Nehrkorn for sharing the Stochastic Time-Inverted Lagrangian Transport (STILT) code and providing advice, Chris Potter and William Salas for sharing modeled CH_4 emission for use as a priori estimates, Larry Hunsaker, Marc Vayssières, Joseph Fischer, and Webster Tassat for sharing CARB CH_4 emissions information, Ying-Kuang Hsu and Patrick Vaca for the operation and data processing of CARB CH_4 monitoring network, and Krishna Muriki for assistance running the Weather Research and Forecasting (WRF) and STILT models on the LBNL-Lawrencium computer cluster. We gratefully acknowledge the National Oceanic and Atmospheric Administration (NOAA) Air Resources Laboratory (ARL) for the use of the Hybrid Single Particle Lagrangian Integrated Trajectory (HYSPLIT) model underlying STILT, and the National Centers for Environmental Prediction (NCEP) for the provision of the North American Regional Reanalysis (NARR) meteorology. We also thank Jean Bogner, Eric Crosson, Guido Franco, Eileen McCauley, and Tony VanCuren for valuable comments. This work was predominantly supported by CARB, with additional support from the California Energy Commission, and the US Department of Energy. Work was completed on May 31, 2012.

TABLE OF CONTENTS

LIST OF FIGURES

LIST OF TABLES

ABSTRACT

We estimate regionally resolved methane (CH_4) emissions for California by comparing CH_4 mixing ratios measured at a network of measurement sites in the Central Valley with transport model predictions based on two independent emission maps: a 0.1 degree seasonally varying "California-specific" emission map, calibrated to state-wide by CH_4 emission totals, and the 0.1 degree global EDGAR42 CH_4 emission map. Atmospheric particle trajectories and surface footprints (sensitivity of CH_4 signals to surface emissions) are computed using the Weather Research and Forecasting (WRF) and Stochastic Time-Inverted Lagrangian Transport (STILT) models. Uncertainties due to wind velocity and boundary layer mixing depth are evaluated using measurements from radar wind profilers. Bayesian region analyses yield annually averaged CH_4 emissions for California totaling 1.2±0.1 and 1.9±0.3 times larger than the current State total CH_4 emissions (32 Tg CO_2 equivalent yr^{-1}) for the California-specific CH_4 and EDGAR42 CH_4 emission maps, respectively, while source analyses estimate slightly higher emissions for both emission models. When emissions from large urban areas are estimated based on a recent study in the larger Los Angeles metropolitan region to better constrain urban emissions, State total CH_4 emissions are estimated to be 1.3 – 1.7 times larger than the current State total CH_4 emissions. These results based on the multiple emission models suggest that the California total of CH_4 emissions would account for approximately 8% - 13% of the State's total greenhouse gas (GHG) emissions, which is significantly higher than the CARB inventory (~6% of total GHG emissions). Spatial resolution of emissions within the influence region reveal seasonality expected from several biogenic sources, including rice agriculture. We expect that additional tower measurements in the South Coast Air Basin will provide the data necessary for a complete analysis of California's CH_4 budget.

EXECUTIVE SUMMARY

Background

Methane (CH_4) is the second highest contributor to climate change among greenhouse gases (GHGs) behind carbon dioxide (CO_2), based on its concentration changes in the atmosphere since the start of the industrial revolution and its ability to absorb infrared radiation. At the regional scale, California currently emits approximately 500 Tg (1 Tg = 1 million metric ton) of CO_2 equivalent (CO_2eq) GHGs, with CH_4 currently estimated to contribute approximately 6% of the total [California Air Resources Board (CARB), 2010].

Methods

This report quantifies regional CH_4 emissions within California with a Bayesian inverse modeling approach, representing the first analysis of CH_4 emissions across a large swath of California and across different seasons using atmospheric observations from multiple sites. The inverse modeling approach follows the approach taken in Zhao et al. [2009], Jeong et al. [2012a] and Jeong et al. [2012b]. We calculate predicted CH_4 signals using two relatively high resolution (0.1 degree) emissions models, a California specific model and the EDGAR4.2 global emission model. Central to this approach, we quantify model-measurement uncertainties by estimating errors in transport variables (e.g., wind velocities and planetary boundary layer depth) that affect footprints (sensitivity of CH_4 signals to surface emissions in units of concentration/flux) and propagating those errors to produce uncertainty in predicted CH_4 signals. The Bayesian inverse analysis then estimates posterior CH_4 emissions for regions (region analysis) and source sectors (source analysis).

Results

This study shows that actual CH_4 emissions based on inverse region analyses are 1.2±0.1 - 1.9±0.3 times larger than the current inventory estimates (32 Tg CO_2eq). When emissions from large urban areas (e.g., Southern California region) are estimated based on a recent study in the larger Los Angeles metropolitan region and combined with the emissions from the Central Valley and other non-urban regions, State total CH_4 emissions are 1.3 – 1.7 times larger than the current State total CH_4 emissions. A Bayesian region analysis suggests that the relatively large range of total emissions reflects a current limitation to uniquely resolve urban versus rural CH_4 emissions, particularly from Southern California. A similar source sector analysis suggests that the dominant CH_4 emissions are derived from livestock and landfills, though as with the region analysis, significant differences are obtained with the California-specific and EDGAR42 prior emission maps.

Conclusions

Atmospheric CH_4 measurements can be combined to estimate total CH_4 emissions at regional scales using the inverse modeling approach. California's CH_4 emissions exceed current inventory estimates, though considerable uncertainty remains. Recommendations for work that will likely resolve these uncertainties include:

- The current GHG network constrains annual average CH_4 emissions from California's Central Valley to be between 26.3±1.8 Tg CO_2eq and 27.4±2.1 Tg CO_2eq for the California-specific and EDGAR42 emission models respectively. Similarly, emissions from livestock (which are predominantly located in the Central Valley) are estimated to be 28.2±3.4 Tg CO_2eq and 25.8±3.2 Tg CO_2eq from the California-specific and EDGAR42 emission models, respectively.

- While significant error reductions are obtained in California's Central Valley, emissions from other regions remain uncertain, with the ratio of emissions to the current California CH_4 emission inventory (32 Tg CO_2eq yr^{-1}) ranging from 1.2±0.1 and 1.9±0.3 from the Bayesian region analysis based on the California-specific and EDGAR42 emission models. Hence, additional tower measurements in the San Francisco Bay and Southern California areas are required to constrain those emissions.

- Noting the large uncertainty in urban emissions estimated from measurements in the Central Valley, emissions from large urban areas (San Francisco Bay Area and Southern California region) are estimated based on a recent study in the larger Los Angeles metropolitan region to better constrain large urban emissions. Combined with the emissions from the Central Valley and other non-urban regions, State total CH_4 emissions are estimated to be 1.3 – 1.7 times larger than the current State total CH_4 emissions where the uncertainty is dominated by uncertainty in the urban regions. This further suggests that additional measurements in the San Francisco Bay and Southern California areas are required to constrain those emissions.

- Data from the current CH_4 measurement network are effective for use in constraining emissions from different regions of California's Central Valley but cannot be used to uniquely attribute emissions to specific source sectors. Additional measurements of source specific tracers (e.g., CO, VOCs, and potentially $_CH_4$ isotopes) will help separate different sources of CH_4.

- Currently, uncertainty in the inverse model estimates of CH_4 emissions for regions containing measurement sites are dominated by uncertainty in the meteorological modeling of trace gas transport (e.g., winter) and estimation of background signals (e.g., summer). Additional work is needed to identify the source of these errors and reduce them.

PROJECT REPORT

1. Introduction

Methane (CH_4) is the second highest contributor to climate change among greenhouse gas (GHG) behind carbon dioxide (CO_2), based on its concentration changes in the atmosphere since the start of the industrial revolution, the long residence time of CH_4 and its ability to absorb infrared radiation. Earth's CH_4 has increased by about 150% since 1750 in concentration, and accounts for ~ 25% of the global total radiative forcing from all long-lived and globally mixed GHGs [Hofman et al., 2006; Montzka et al., 2011]. Given the importance of CH_4 as a GHG it is important to be able to quantify changes in emissions. However, there exists a large uncertainty in bottom-up emission inventory models that take known natural and anthropogenic sources of CH_4 to produce emission estimates due to lack of understanding of emission processes and driving data. Mathematical inversion models, which use concentration changes in CH_4 and transport to infer sources, provide an effective tool for understanding CH_4 emissions. Correspondingly, attention has focused on inverse model assessment of global [Gimson and Uliasz, 2003; Houweling et al., 1999; Miller et al., 2008], and regional [Kort et al., 2008; Zhao et al., 2009; Jeong et al., 2012a] CH_4 sources.

At the regional scale, California currently emits approximately 500 Tg (1 Tg = 1 million metric ton) of CO_2 equivalent GHGs, with CH_4 currently estimated to contribute approximately 6% of the total [California Air Resources Board (CARB), 2011]. Because California has committed to an ambitious plan to reduce GHG emissions to 1990 levels by 2020 through Assembly Bill 32 (AB-32), verifying the success of control strategies will require accounting for CH_4 emissions.

This report quantifies regional CH_4 emissions from California within a Bayesian inverse modeling framework, representing the first analysis of CH_4 emissions in California using atmospheric observations from multiple sites across different seasons during 2010 - 2011. The work expands on studies by Zhao et al. [2009] and Jeong et al. [2012a] that quantified CH_4 emissions from central California using a single tower near Walnut Grove, California (WGC). In Section 2, we describe the methods we employed, including atmospheric measurements, *a priori* CH_4 emissions inventories, mesoscale meteorology and trajectory transport modeling, and the Bayesian inverse method. Section 3 describes results, including the seasonal variations in calculated footprints, and the inferred surface emissions of CH_4 from California for different regions and sources based on simple correlation analysis and a Bayesian inverse analysis. Section 4 summarizes the results and presents the recommendations for CH_4 inverse modeling at the regional scale, highlighting the importance of uncertainty in the spatial distribution of *a priori* emissions, and the value of multiple measurement stations.

2. Approach

The inverse modeling framework used in this study follows the approach taken in Zhao et al. [2009], Jeong et al. [2012a] and Jeong et al. [2012b]. As illustrated in Figure 1, the Bayesian inverse model requires two direct inputs: 1) tower measurements, and 2) predicted signals. By comparing the measured signals at the tower with predicted signals, the inverse model estimates scaling factors for surface emissions such that the scaled surface emissions yield predicted signals that are statistically consistent with measurements. Predicted signals are calculated as a linear combination of footprints, which represent the sensitivity of signals measured at different sites to emissions across the landscape, and surface emissions. Because predicted signals represent local enhancements of emissions, background signals entering the study domain are needed to compare predicted signals with measured signals, which include both local and background signals. Footprints are quantified using a Lagrangian model for air parcels arriving at a tower. Such footprints link the observed concentrations at a specific location and height to surface fluxes within a large area. Numerical model outputs are used to define paths traveled by parcels of air, or trajectories, which are a basis for footprint estimates. In this study we use the coupled WRF-STILT model for trajectory calculations. Errors in modeling footprints due to uncertainties in winds and planetary boundary layer (PBL) heights contribute to uncertainties in inversion results and confidence levels associated with optimized emissions values. The result of the Bayesian inverse model is a set of optimized scaling factors for region or source emissions.

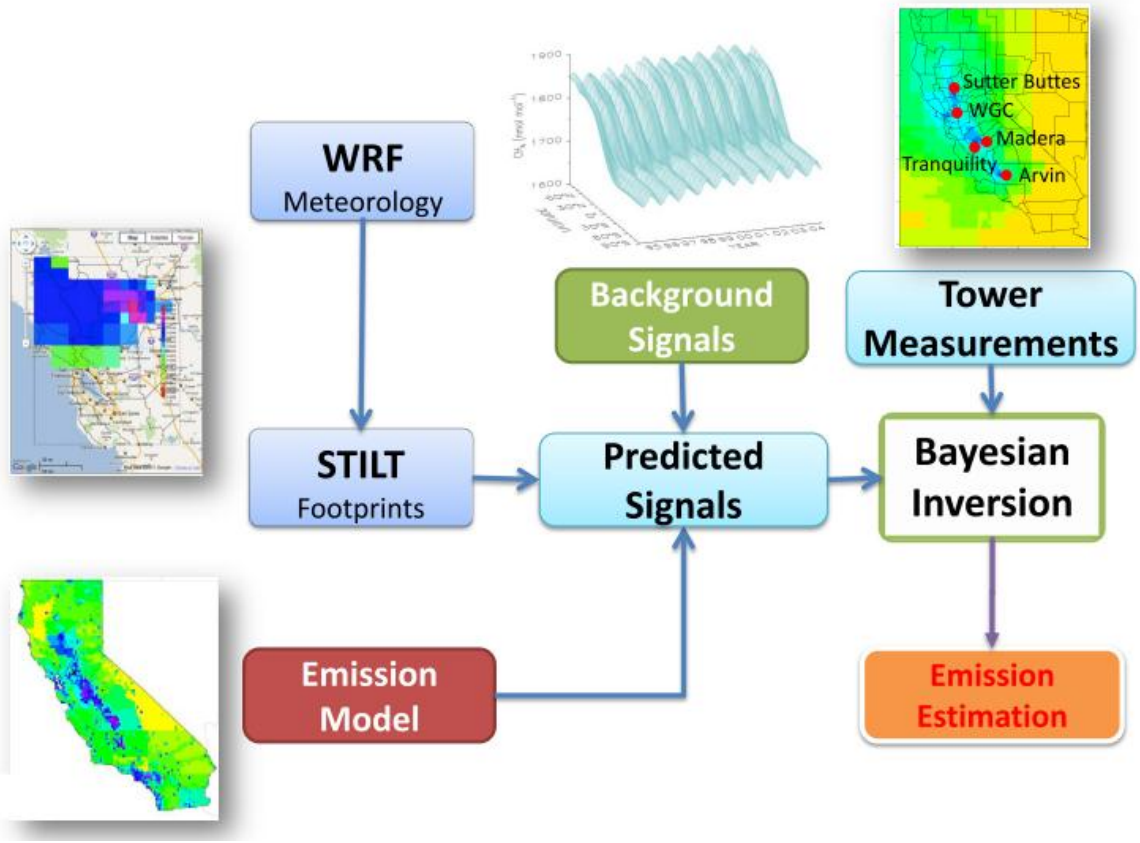

Figure 1. Inverse modeling approach used in the study.

2.1. CH_4 Measurements and Boundary Conditions

CH_4 measurements were made at the collaborative five-site GHG network in California's Central Valley. In addition to the Central Valley sites, CH_4 measurements were also made at Mt. Wilson, but these measurements are not employed in this study because we have not developed a well-tested meteorological model for atmospheric transport at Mt. Wilson at this time. Table 1 summarizes the information for the measurement sites in the measurement network and the measurement periods used in the inverse analysis. The Arvin (ARV) site is located at the southern end of the San Joaquin Valley and constrains emission sources from livestock, and gas and petroleum production fields. The Madera (MAD) and Tranquility (TRA) sites are located in the center of the San Joaquin Valley, constraining emission sources mainly from livestock. The Sutter Butte site located in the Sacramento Valley represents an emission region that has dominant CH_4 emissions from rice agriculture. As described in detail in Zhao et al. [2009] and Jeong et al. [2012a], the site represents an emission region with mixed CH_4 emission sources such as crop agriculture, livestock, natural gas fields, wetlands and urban emissions.

CH_4 measurements at WGC were made at 91 and 483 m above ground level on a tall tower, beginning in September 2007. The CH_4 mixing ratios at each height are measured every 15 minutes and averaged into the 3-hour means used in this study. As in Zhao et al. [2009] and Jeong et al. [2012a], CH_4 measurements at 91 m are used for inverse modeling. Detailed information about these measurements is described by Zhao et al. [2009] and Jeong et al. [2012a]. All other stations are measured at 10 meters above the ground using the same type of instruments and calibrated with standard gases from NOAA every six months. Each instrument is programmed to measure from precision check standard gases every 11 hours to ensure data quality. After examining precision checks and removing special events (e.g., changing filters), raw data collected every few seconds are averaged into 3-hourly measurements for inverse modeling.

Table 1. Measurement Sites and Periods

Site Name	Height[a]	Elevation[b]	Latitude	Longitude	Measurement Period (yyyymm)
Arvin (ARV)	10 m	158 m	35.24°N	118.79°W	201009 - 201106
Madera (MAD)	10 m	81 m	36.87°N	120.01°W	201009 - 201106
Sutter Butte (STB)	10 m	640 m	39.21°N	121.82°W	201105 - 201106
Tranquility (TRA)	10 m	59 m	36.63°N	120.38°W	201009 - 201106
Walnut Grove (WGC)	91 m	0 m	38.27°N	121.49°W	201009 - 201106

[a]Above ground level (a.g.l.)
[b]Above sea level (a.s.l.)

CH_4 boundary values were estimated using data from the Pacific coast aircraft network CH_4 profiles (http://www.esrl.noaa.gov/gmd/ccgg/aircraft/) and remote Pacific marine boundary layer sampling sites (http://www.esrl.noaa.gov/gmd/ccgg/flask.html) within the NOAA ESRL Cooperative Air Sampling Network. The data were smoothed and interpolated to create a three-dimensional (3-D) curtain, varying with latitude, height and time. As in Zhao et al. [2009]

and Jeong et al. [2012a], predicted background values are computed for each footprint simulation by sampling the curtain at each of the 500 STILT trajectory endpoints and calculating the average value.

Figure 2 shows the measured CH_4 at each of the five sites and the predicted background signals based on the 3-D curtain. For inverse analysis, the hourly measurements and predicted background signals are aggregated into 3-hourly time periods as in Jeong et al. [2012a]. Unlike WGC, the other sites do not have multiple measurement levels. Therefore, it is difficult to identify well-mixed periods without using vertical CH_4 gradients from multiple-level measurements. In this study, we use data during day time (noon to afternoon) when vertical mixing is strong. In general, the variability in measured CH_4 is larger in winter than the other seasons for most of the sites. However, the MAD site shows high variability during all seasons although spring and summer seasons show slightly smaller variability than fall and winter. As stated earlier, the MAD site constrains regions where dairy emissions are large. In addition, the minimum measured signals approximate the predicted background CH_4, suggesting that the estimated background signals are reasonable and there is no significant bias in the measured signals.

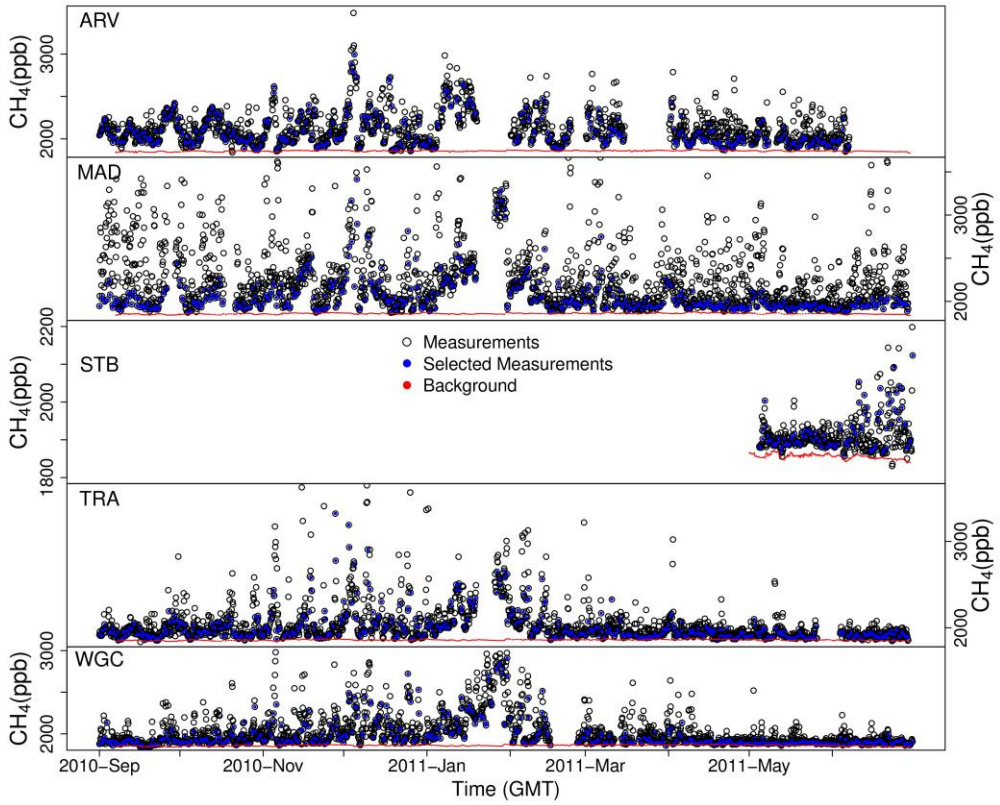

Figure 2. Measurements of CH_4 from the five sites and WRF-STILT predicted CH_4 background signals using the 3-D curtain for the period between September 2010 and June 2011. The black circles show 3-hourly measurements during the entire analysis period. The filled blue circles indicate data measured during noon-afternoon hours (12 – 17, local time), which are used for the inverse study, and the red line shows predicted CH_4 background signals.

2.2. A priori CH_4 Emission Maps

This work adopts the *a priori* CH_4 emission model from Jeong et al. [2012a], which provides a high spatial resolution ($0.1^o \times 0.1^o$) for California and has seasonal components for wetlands and crop agriculture. As described in Jeong et al. [2012a], the high resolution emission model was prepared by scaling to the CARB inventory by sector [CARB, 2010]. The considered sectors include: crop agriculture (CP), landfills (LF), dairy livestock (DLS), non-dairy livestock (NDLS), natural gas (NG), petroleum (PL), wastewater (WW), and wetlands (WL). Figure 3 shows California-specific CH_4 emission maps for sectors without temporal variation.

Because there is no specific emission estimate for wetlands from CARB, wetland CH_4 emissions are taken from monthly averages of the Carnegie-Ames-Stanford-Approach CH_4 (CASA-CH_4) model from Potter et al. [2006]. Also, seasonally varying CH_4 emissions for CP CH_4 sources were taken from the denitrification and decomposition model (DNDC) output (assuming the 1983, high irrigation case) described by Salas et al. [2006]. Monthly averaged CH_4 emission maps for county level agricultural CH_4 fluxes are used. The temporally-varying emission maps for CP and WL are averaged annually and shown in Figure 4. Table 2 summarizes the annual mean CH_4 emissions for the California-specific model by region and sector. In this study, CH_4 emissions are scaled to CO_2 equivalent using a 100-year global warming potential (GWP) of 21 g CO_2 eq / g CH_4 [IPCC, 1995].

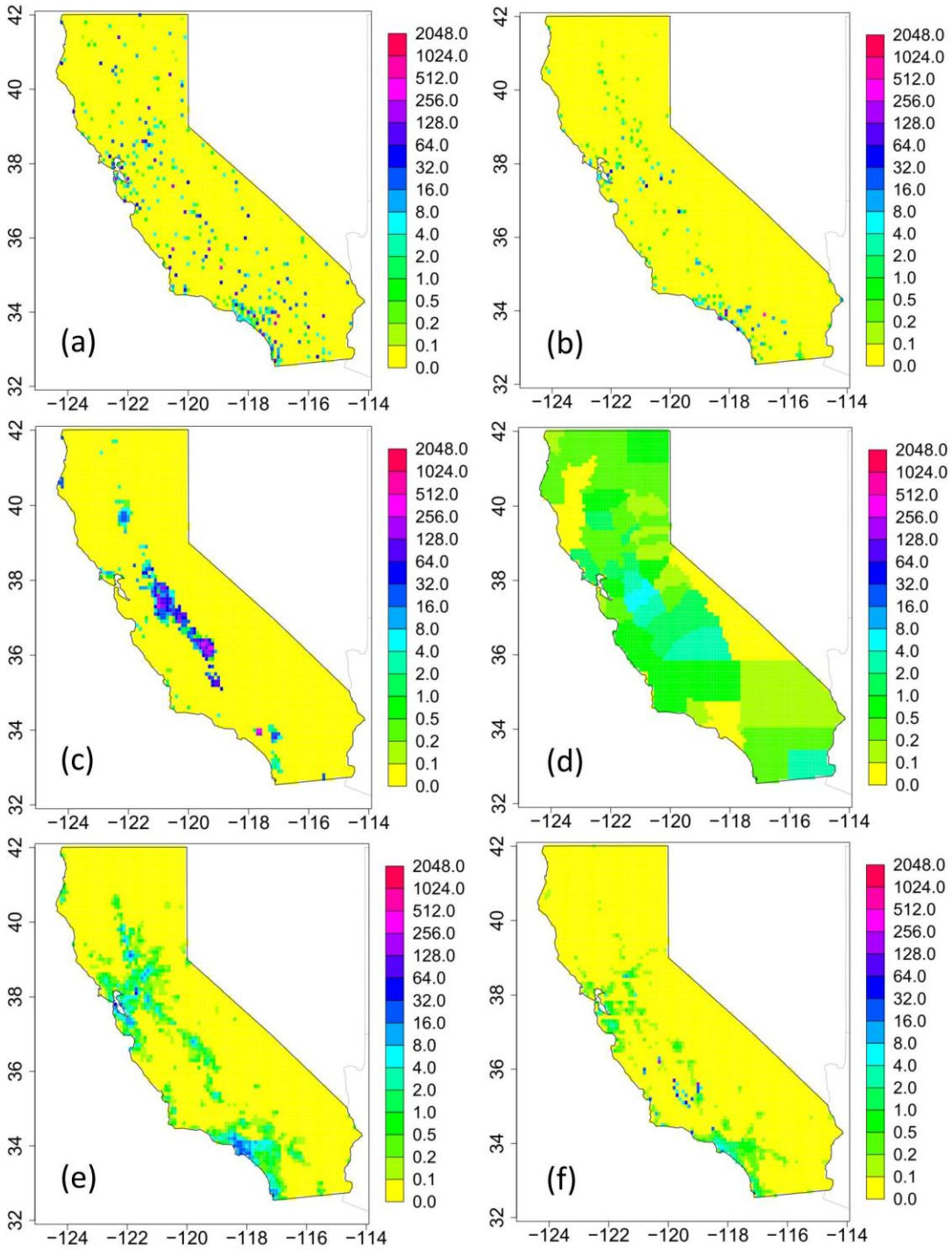

Figure 3. California-specific CH_4 emission maps for source sectors: (a) LF, (b) WW, (c) DLS, (d) NDLS, (e) NG, and (f) PL.

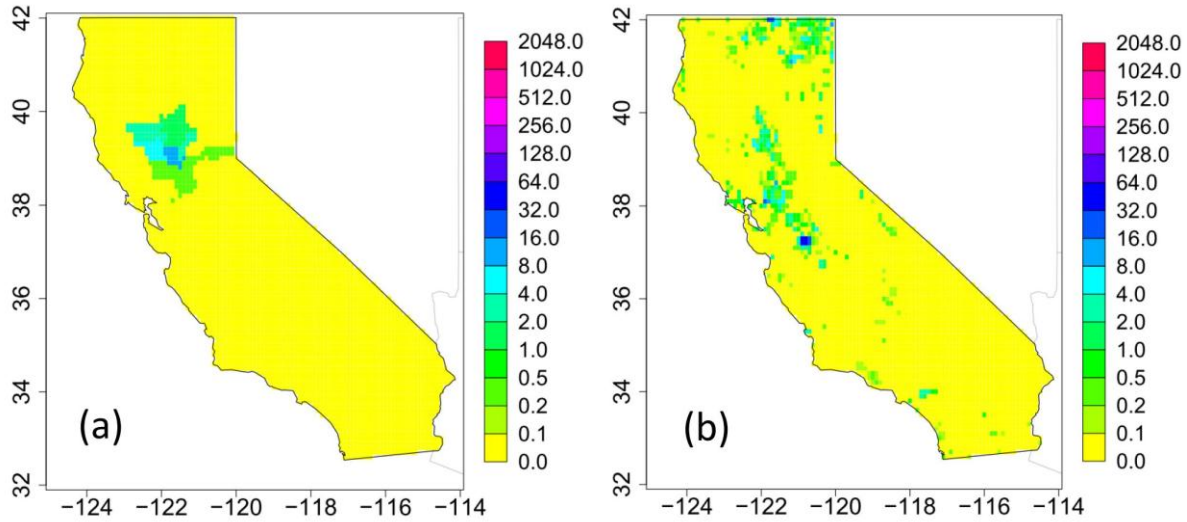

Figure 4. California-specific CH_4 emission maps for source sectors that have seasonal components: (a) CP and (b) WL.

Table 2. Annual Average California-specific CH_4 Emissions by Region and Sector (Tg CO_2eq)

	R01	R02	R03	R04	R05	R06	R07	R08	R09	R10	R11	R12	R13	Sector Total
CP	0.00	0.00	0.00	0.01	0.00	0.50	0.00	0.01	0.00	0.00	0.01	0.00	0.02	0.54
LF	0.12	0.08	0.18	0.18	0.23	0.31	0.48	0.33	0.64	3.05	0.07	0.95	0.08	6.69
DLS	0.00	0.00	0.01	0.10	0.01	0.36	0.08	3.79	0.02	1.71	0.03	5.77	0.01	11.90
NDLS	0.03	0.10	0.11	0.06	0.17	0.19	0.12	0.54	0.11	0.64	0.07	1.00	0.03	3.17
NG	0.00	0.01	0.04	0.02	0.01	0.33	0.33	0.10	0.05	0.91	0.02	0.11	0.03	1.95
PL	0.00	0.00	0.05	0.00	0.00	0.03	0.05	0.02	0.07	0.19	0.00	0.71	0.00	1.13
WW	0.00	0.09	0.02	0.01	0.00	0.03	0.17	0.08	0.06	1.33	0.01	0.11	0.01	1.92
WL	0.01	0.00	0.00	0.00	0.22	0.18	0.03	0.27	0.01	0.03	0.01	0.02	0.01	0.79
Total	0.16	0.28	0.41	0.40	0.65	1.92	1.26	5.14	0.96	7.85	0.21	8.68	0.18	28.09

The EDGAR42 (European Commission Joint Research Centre (JRC) and Netherlands Environmental Assessment Agency, Emission Database for Global Atmospheric Research (EDGAR), release version 4.2, 2011, http://edgar.jrc.ec.europa.eu) CH_4 emission model also provides high-resolution emission maps and its estimates are compared with estimates from the California-specific model in Figure 5. Compared with the California-specific model, EDGAR42 generally shows a similar spatial distribution of CH_4 emissions. However, EDGAR42 shows larger emissions in urban areas than the California-specific model. For the Central Valley, the California-specific model shows higher emissions than EDGAR42, mainly due to the higher estimates of dairy emissions. Figure 5d shows the sub-region classification described in Zhao et al. [2009] and Jeong et al. [2012a]. The sub-regions were defined by considering the emission sources and measurement sites, and roughly follow the California Air Basins. Emissions from these regions are adjusted by the corresponding scaling factors estimated by the inverse model.

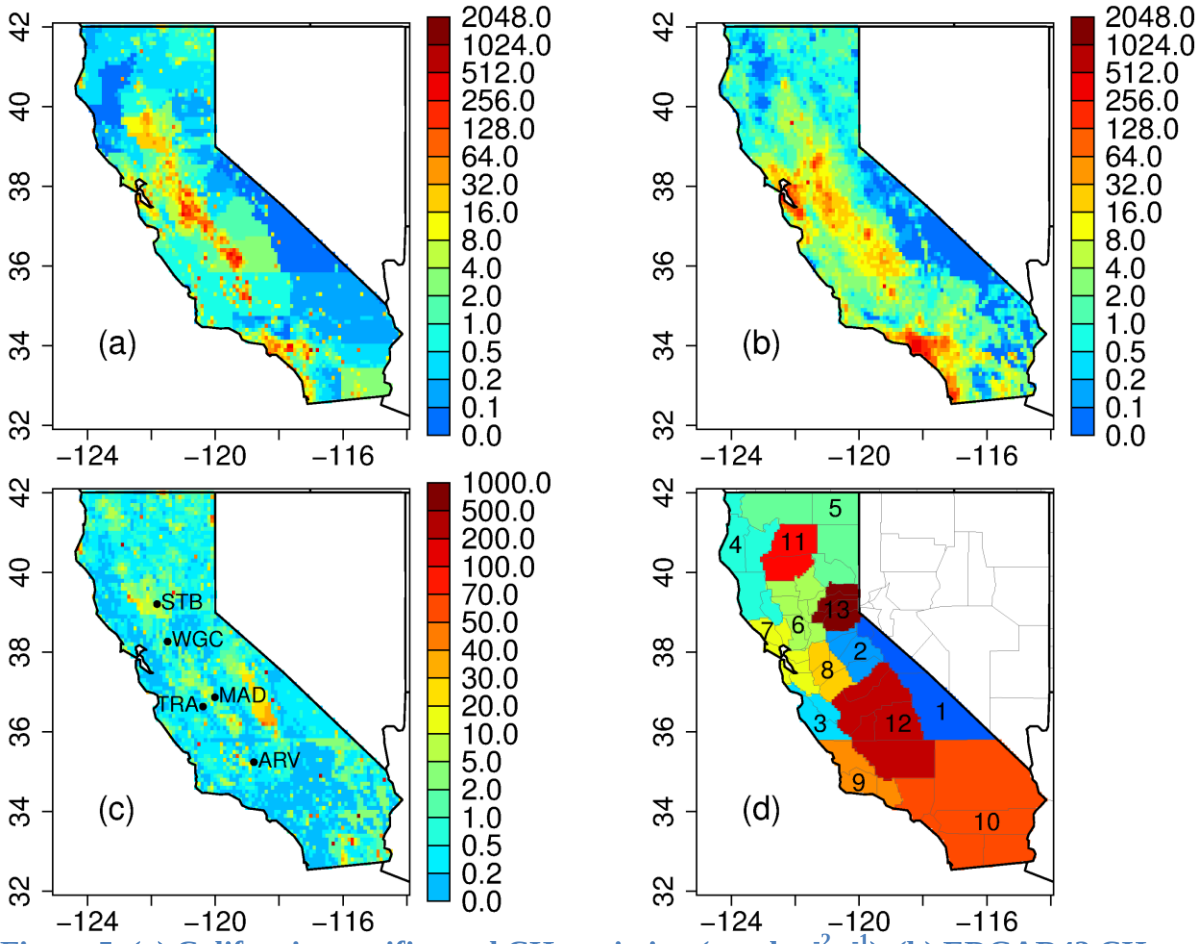

Figure 5. (a) California-specific total CH_4 emission (nmol m^{-2} s^{-1}), (b) EDGAR42 CH_4 total emission (nmol m^{-2} s^{-1}), (c) the ratio of California-specific CH_4 to EDGAR42 CH_4, and (d) sub-region classification for the inverse analysis.

Figure 6 shows the comparison between the California-specific and EDGAR42 emissions by region. As can be seen in the figure, EDGAR42 shows more weight in urban areas than the California-specific model. For example, for Regions 7 and 10, which include San Francisco Bay Area and the Southern California Air Basin, respectively, EDGAR estimates significantly higher CH_4 emissions than the California-specific model. Currently, Region 10 is a single large sub-region due to relatively weak sensitivity from the measurement sites in the Central Valley. However, Region 10 needs to be divided into smaller sub-regions when more measurements sites are available in the region. As shown in the emission maps, the California-specific model estimates higher emissions than EDGAR in Region 8 where dairy is a dominant emission source (more than 80%). The annual total emission for California from the California-specific model and the EDGAR42 model is 28.1 and 38.3 Tg CO_2eq, respectively. As described in Jeong et al. [2012a], the California-specific model is scaled to the 2008 statewide total CH_4 emissions contained in the CARB CH_4 emission inventory by sector [CARB, 2010]. Table 3 shows the comparison of CH_4 emissions by source between the CARB inventory and the EDGAR42 emission model.

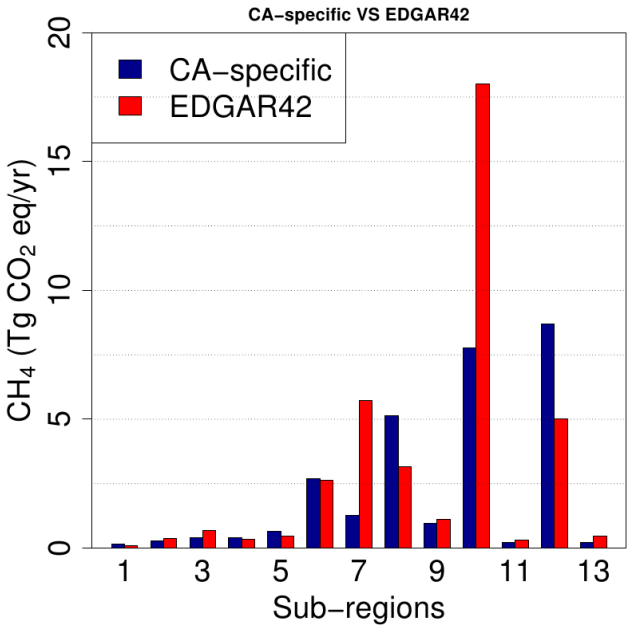

Figure 6. Comparison between the California-specific and EDGAR42 emissions by region

Table 3. Comparison of CH_4 Emissions by Source between CARB Inventory and EDGAR42 Emission Model

CARB Category	CARB Emission (Tg CO_2eq)	EDGAR42 Category	EDGAR42 Emission (Tg CO_2eq)
Rice crop area	0.5	Agricultural soils	0.7
Landfill	6.7	Solid waste	12.7
Dairy cows	11.9	Enteric fermentation	7.3
Non-dairy cows	3.2	Manure management	2.4
Natural gas pipeline	1.9	Gas production and distribution	10.2
Extraction, mobile, refining	1.1	Oil production and refineries	0.5
Wastewater treatment	1.9	Waste water	3.2
Others	1.2		1.4
CARB Total	28.5	EDGAR Total	38.3

2.3. Atmospheric Transport Modeling

Predicted contributions to CH_4 mixing ratios from emissions within the modeling domain are calculated as **FE**, where **F** is footprint strength, and **E** is the *a priori* CH_4 emissions. Footprints represent the sensitivity of the mixing ratio at the receptor location to surface sources, in units of ppb/(nmol m^{-2} s^{-1}). Footprints are calculated from particle trajectories simulated using the STILT model [Lin et al., 2003, 2004]. As in Jeong et al. [2012a], 500 particles are released hourly at each measurement site and transported backward in time 7 days to ensure that the majority of the particles reach positions representative of the upwind boundary conditions. The meteorology

used to drive this transport model is from the simulation of Weather Research and Forecasting (WRF3.2.1) model [Skamarock et al., 2008]. The WRF model has been slightly modified to be coupled with STILT (WRF-STILT) by Nehrkorn et al. [2010].

The WRF model simulations closely follow those described in Jeong et al. [2012a] with the following modifications. Five domains (d01 – d05) of 36, 12, 4, and two 1.3 km resolution were used in the WRF simulations. The 4-km domain (i.e., d03) was configured to represent most of California with the two 1.3-km nested domains (d04 and d05) that cover the San Francisco Bay Area and the metropolitan area of Los Angeles, respectively. In this study, we used the meteorology within the d01, d02 and d03 domains to drive the STILT model. We did not include the 1.3-km resolution domains because the GHG measurement sites are located in the Central Valley. Figure 7 shows the WRF d01, d02, and d03 domains used in this study. The simulations were run with two-way nesting instead of one-way nesting used in Jeong et al. [2012a]. As in Jeong et al. [2012a], 50 vertical levels were employed to resolve PBL heights over complex terrain features of California. Initial and boundary meteorological conditions were provided by the North American Regional Reanalysis (NARR) dataset [Mesinger et al., 2006]. All simulation durations were 30 hours allowing for 6 hours of model spin up and 24 hours of forecast time. The model also incorporated 3-D analysis nudging every three hours in the 36-km domain.

As in Jeong et al. [2012a], the Mellor-Yamada-Janjic (MYJ) scheme [Mellor and Yamada, 1982; Janjić, 1990] was used for the PBL scheme. However, we found that the Yonsei University (YSU) scheme performs better than the MYJ scheme for some months depending on the wind profiler site. For example, the WRF simulations for PBL heights based on the YSU scheme agreed with wind profiler measurements better than those of the MYJ scheme at the Lost Hills site. Therefore, we used the YSU scheme for the cases where YSU simulations are more comparable with measurements than those of the MYJ scheme.

The land surface model provides heat and moisture fluxes over land and sea-ice that provide crucial information for the PBL schemes and other atmospheric processes to accurately predict transport. These land surface models provide the lower boundary conditions for the PBL schemes and can have a considerable effect on the boundary layer physics. This study examined two different land surface models (LSM), the Noah LSM and the five-layer thermal diffusion scheme LSM (5-L LSM hereafter) to evaluate the models in terms of PBL and wind simulations. The Noah LSM uses four soil layers with thicknesses of 10 cm, 30 cm, 60 cm, and 100 cm from the top down. It includes vegetation processes, estimates of soil temperature, soil moisture, and canopy moisture. Compared to the Noah LSM, the 5-L LSM is a simpler LSM that uses five soil layers with thicknesses of 1 cm, 2 cm, 4 cm, 8 cm, and 16 cm from the top down [Skamarock et al., 2008]. It uses a static soil moisture estimate that is a function of land use and season. We found that in general the 5-L LSM performs better than the Noah LSM during those months when irrigation is significant in the Central Valley. This is likely related to the deficiency of the Noah LSM in describing the irrigation component. Depending on the performance, we choose the best LSM for a given season.

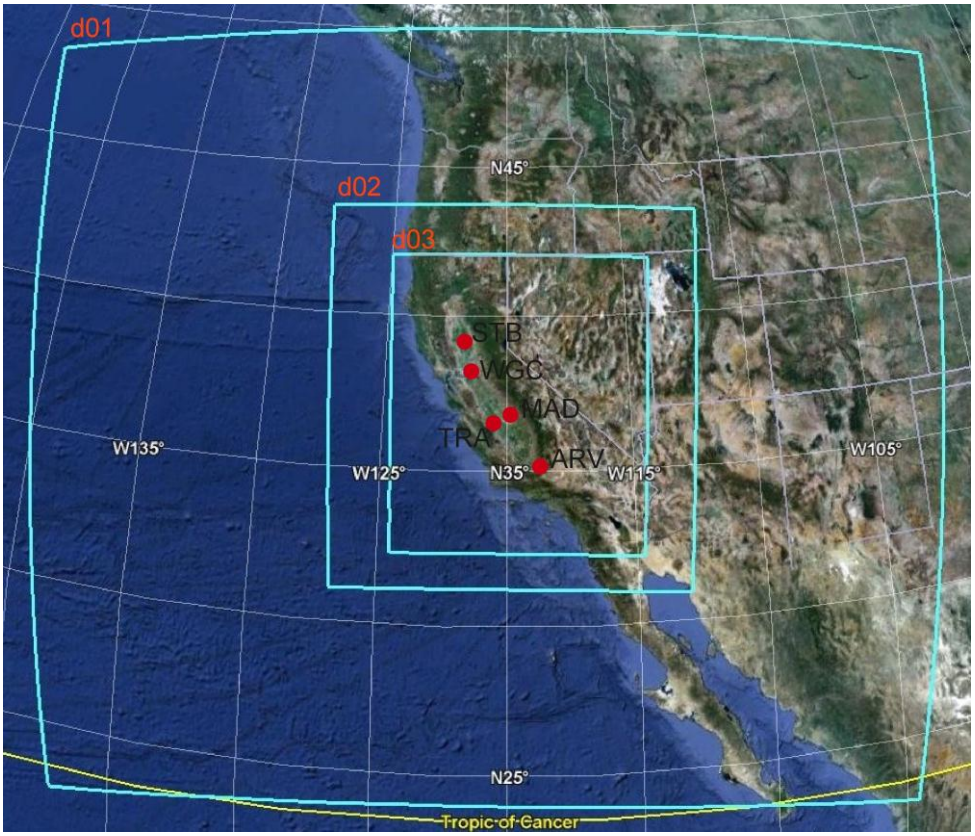

Figure 7. WRF modeling domain configuration with three-level nested domains (d01, d02, and d03 featuring 36, 12, and 4 km resolution, respectively).

2.4. Bayesian Inverse Model

Seasonally varying regional (~10,000 km^2) CH_4 emissions from California's Central Valley are estimated by scaling high-resolution (~10 km) CH_4 emission maps using a Bayesian inversion model to provide optimal agreement with aggregate mixing ratio data measured at the five-site network. This inversion approach expands on the earlier efforts by Zhao et al. [2009], Jeong et al. [2012a] and Jeong et al. [2012b], which used measurements from the WGC site to constrain GHG emissions from central California. As described in Gerbig et al. [2003], Lin et al. [2003], Zhao et al. [2009], and Jeong et al. [2012a], the local CH_4 mixing ratio at the receptor (**c)** can be modeled as

$$\mathbf{c} = \mathbf{K}\boldsymbol{\lambda} + \mathbf{v}, \qquad (1)$$

where $\mathbf{K} = \mathbf{FE}$, $\boldsymbol{\lambda}$ is a state vector for scaling factors, which is used to adjust emissions from sources or regions, and **v** is a vector representing the model-data mismatch with a covariance matrix **R**. We model **R** as a diagonal matrix to represent the total variance associated with all error sources such as the measurement error and the transport error. Following the Gaussian assumptions, the posterior estimate for $\boldsymbol{\lambda}$ is

$$\boldsymbol{\lambda}_{post} = \left(\mathbf{K}^T\mathbf{R}^{-1}\mathbf{K} + \mathbf{Q}_{\lambda}^{-1}\right)^{-1}\left(\mathbf{K}^T\mathbf{R}^{-1}\mathbf{c} + \mathbf{Q}_{\lambda}^{-1}\boldsymbol{\lambda}_{prior}\right) \qquad (2)$$

where $\boldsymbol{\lambda}_{prior}$ is the *a priori* estimate for $\boldsymbol{\lambda}$, and $\mathbf{Q}_{\lambda}$ is the error covariance associated with $\boldsymbol{\lambda}_{prior}$. The corresponding posterior covariance for $\boldsymbol{\lambda}$ is $\mathbf{V}_{post} = \left(\mathbf{K}^T\mathbf{R}^{-1}\mathbf{K} + \mathbf{Q}_{\lambda}^{-1}\right)^{-1}$. To determine optimal emissions, we use the inversion method at a monthly temporal scale based on the two CH_4 *a priori* emission models. Because the measurements sites are located in California's Central Valley that includes such uncertain CH_4 emission sources as rice agriculture, livestock and natural gas fields, we use 50% uncertainty in our *a priori* emission models as in Jeong et al. [2012a]. The inverse modeling approach is applied in two phases as in Bergamaschi et al. [2005] and Jeong et al. [2012a]. After a first inversion, the second (final) inversion uses data points that are accepted by applying the selection criteria $|\mathbf{c}_i - (\mathbf{K}\boldsymbol{\lambda})_i|^2 < \alpha\mathbf{R}_i$, where α is a fixed value. As in the first inversion, the final inversion is performed using the original *a priori* emission maps, and therefore the first inversion is used as a data selection tool for the atmospheric observations.

2.5. Uncertainty Analysis

The uncertainty in the model-measurement differences control the relative weighting of the prior flux estimates and the measured data in the inversion, adjusting posterior CH_4 emissions relative to *a priori* emissions. Following Gerbig et al. [2003], Zhao et al. [2009], Göckede et al. [2010], and Jeong et al. [2012a], the model-measurement uncertainty matrix, **R**, is represented as the linear sum of uncertainties from several sources:

$$\mathbf{R}_i = \mathbf{S}_{part} + \mathbf{S}_{aggr} + \mathbf{S}_{bkgd} + \mathbf{S}_{TransPBL} + \mathbf{S}_{TransWIND}, \qquad (4)$$

where the particle number error (S_{part}) is due to the finite number of released particles at the receptor location while the aggregation error (S_{aggr}) arises from aggregating heterogeneous fluxes within a grid cell into a single average flux. The background error (S_{bkgd}) is due to the uncertainty in estimating the background contribution to the CH_4 measurements at the receptor. $\mathbf{S}_{TransPBL}$ and $\mathbf{S}_{TransWIND}$ represent the uncertainty in CH_4 mixing ratios caused by the errors in wind speeds and directions, and the errors in PBL heights, respectively. For the aggregation error ($\mathbf{S}_{aggr}$), we adopt the result from Jeong et al. [2012a] and use 11% of the background-subtracted mean signal.

The background error ($\mathbf{S}_{bkgd}$) is estimated by combining (in quadrature) the RMS error in the estimation of the 3-D curtain and the standard deviation of 500 WRF-STILT background samples, which were calculated as an average for each month. Only time points for which more than 80% of the particles reached the western boundary of the domain were included in the study.

To estimate the uncertainty in predicted CH_4 signals due to errors from modeled PBL heights ($\mathbf{S}_{TransPBL}$) and winds ($\mathbf{S}_{TransWIND}$), we evaluated model errors in winds and PBL heights and then calculated the RMS difference in CH_4 signals obtained from simulations with and without input of an additional stochastic component of wind and PBL errors in STILT. We evaluated PBL heights (*Zi*) and winds at four stations shown in Figure 8. Wind and PBL height measurements from the closest profiler to the GHG measurement site are used to evaluate WRF simulations. For example, most relevant to the ARV GHG measurement site, we compare *Zi* from WRF-STILT with measurements from the LSH profiler. As in Jeong et al. [2012a], we assume that the RMS scatter in predicted versus measured *Zi* can be represented as the sum of squares of

measurement uncertainty [~ 200 m, Dye et al., 1995] and WRF-STILT model uncertainty. As an example of the performance of the WRF model used in this study, Figure 9 shows the *Zi* comparison result between profiler measurements and predictions from WRF for the month of June. Due to the availability of profiler data, the comparison is made for daytime only. In general, the WRF simulated *Zi* is consistent with the measured *Zi*. Although the fitting slope for the CCO site is slightly higher than unity, the diurnal cycle of *Zi* (not shown) suggests that there is no significant bias.

Uncertainty in modeled CH_4 signals due to errors in modeled winds is estimated using modeled and measured winds from the wind profiler. As in the case of *Zi*, the wind error for a given GHG site was evaluated using the nearby profiler winds. Depending on the season and measurement location, the wind error varies ranging from 2 – 5 m s^{-1}, without significant biases. In this study we run the STILT model 10 times and compute ensemble signals for a given site and month to estimate the combined uncertainty due to both wind ($\mathbf{S}_{\mathrm{TransWIND}}$) and particle number ($\mathbf{S}_{\mathrm{part}}$) errors. Based on 10 ensemble runs, we estimate the RMS difference about the mean of the ensemble signals for each model time step and use the average RMS for the combined uncertainty due to wind and particle number errors. Propagating a random wind component of the velocity error through STILT yielded a typical signal variation of ~ 10 % of the background-subtracted mean CH_4 signal.

Following Zhao et al. [2009] and Jeong et al. [2012a], we assumed that all of the errors are independent. The errors were combined in quadrature to yield a total expected model-data mismatch error. The uncertainty in the inverse model estimates of CH_4 emissions for regions containing measurement sites are dominated by uncertainty in the meteorological modeling of trace gas transport (e.g., winter) and estimation of background signals (e.g., summer). Depending on the month and measurement location, the error ranged from 30 – 60% of the background-subtracted mean signal.

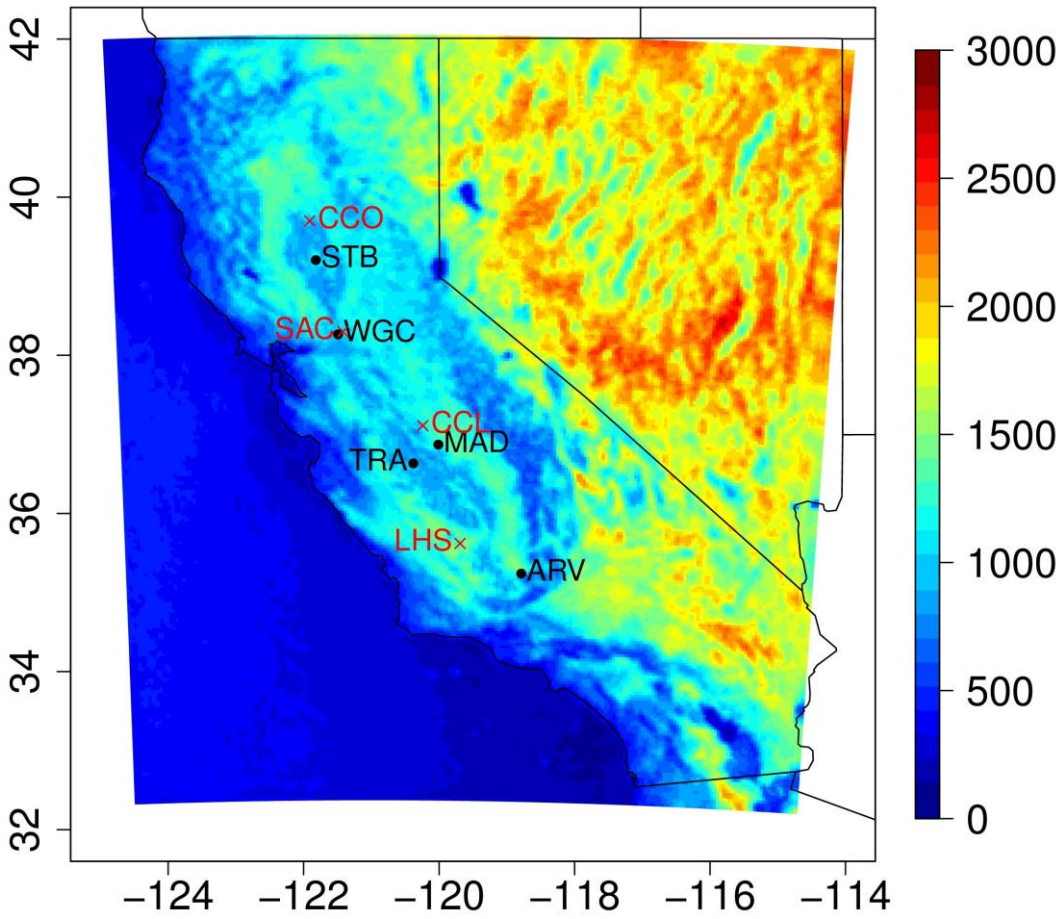

Figure 8. Location of GHG measurement sites (black) and wind profiler sites (red) in the Central Valley with predicted monthly mean PBL heights (m) for June 2011, 14:00 LST shown in color.

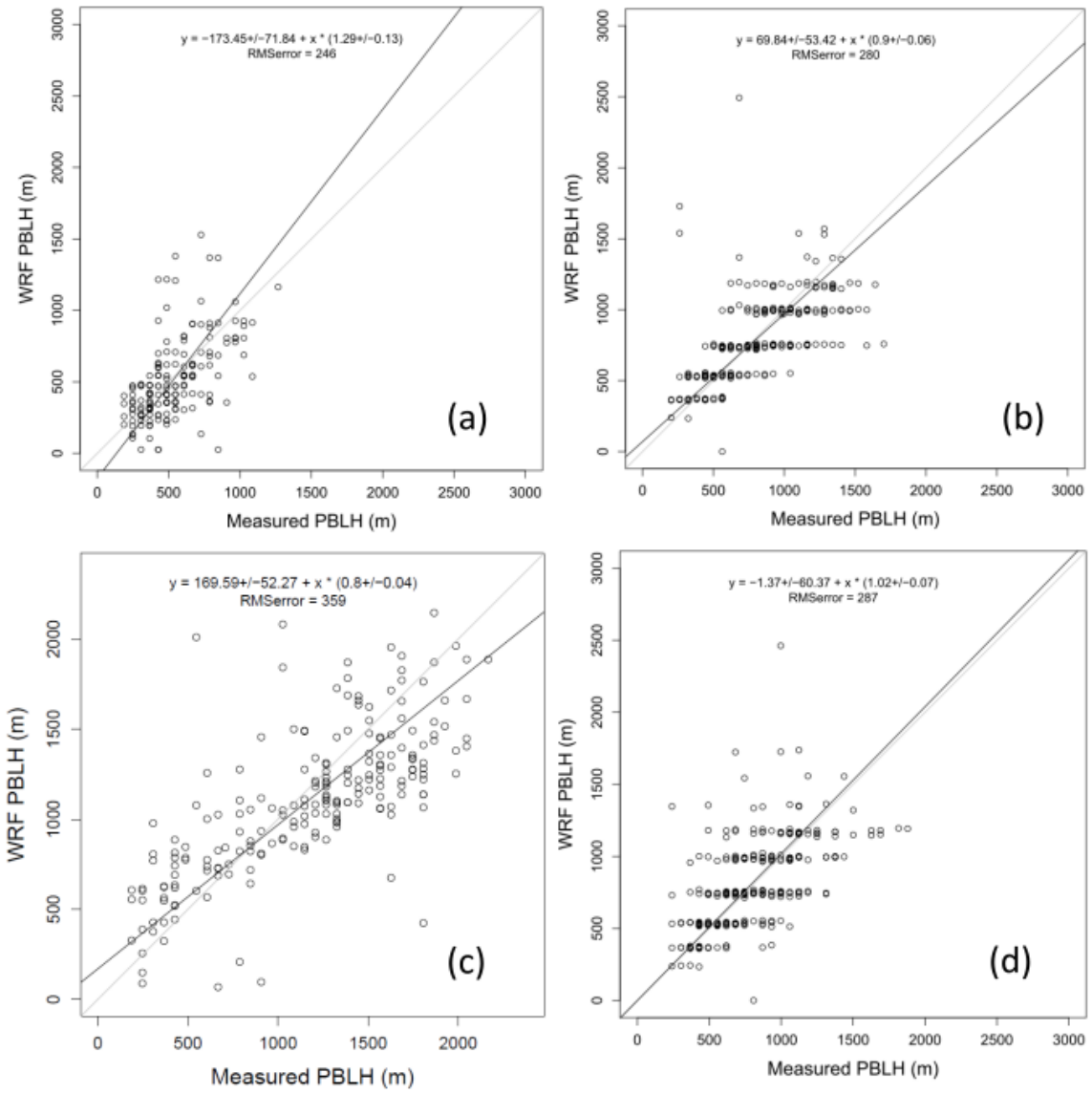

Figure 9. Comparison of measured and predicted *Zi* during the month of June for (a) CCO, (b) CCL, (c) LSH, and (d) SAC. For CCO, data from June 2011 data are used while the other sites use data from June 2010. For this summer month, the 5-L LSM scheme was used for all sites. In terms of the PBL scheme, the MYJ scheme was used for all sites except for LSH where the YSU scheme was used.

3. Results and Discussion

3.1. CH_4 Mixing Ratio

Figure 10 shows the 3-hourly background-subtracted CH_4 mixing ratios and initial predictions using the *a priori* CH_4 emissions for the five network sites. This figure shows the predicted mixing ratios for the well-mixed periods which are used for inverse analyses. Overall, the predicted signals at all sites show underestimation of CH_4 compared to the measurements

although the prediction captures the synoptic variability of the measured signals. Also, the daytime comparison between the predicted and measured signals is shown in Figure 11. The result during the daytime suggests that there is a clear seasonal variation in CH_4 signals with high variability in winter. The CH_4 predictions at ARV are more consistent with the measurements than at the other measurement sites. It is likely due to the fact that the footprints contributing to ARV cover areas with CH_4 emissions from dairy livestock and oil and gas extractions, for which the California-specific emission model estimate significantly higher emissions compared to EDGAR42. Note that, based on the California-specific model, the CH_4 emission sum for Region 12, which includes ARV, is ~1.7 times higher than that of EDGAR42. This suggests that emission estimates for Region 12 from both emission models are low. The comparison result in STB indicates that late spring and summer emissions from rice agriculture are significantly lower than actual emissions. The DNDC model suggests that CH_4 emissions from rice agriculture in Region 6 become strong starting in June with an emission sum of 3.4 Tg CO_2eq yr^{-1} and peaking in August with emissions equating to 4.6 Tg CO_2eq yr^{-1}. For WGC, the predicted signals are significantly lower than the measurements, showing similar results to those shown in Jeong et al. [2012a].

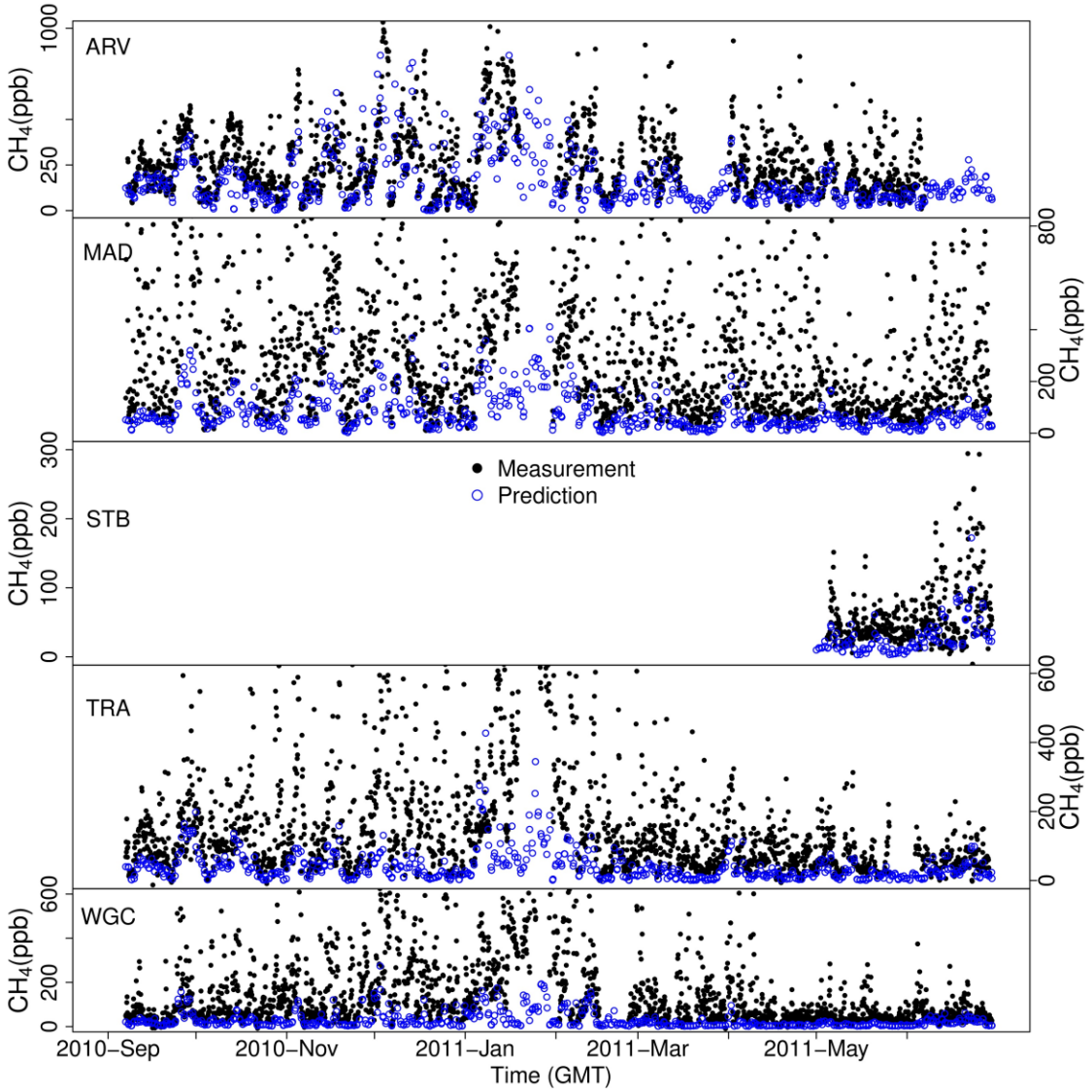

Figure 10. Time series of measured and predicted mixing ratios at the five network sites during September 2010 – June 2011. The measurements are shown for both day and night times while the predictions are shown for only noon-afternoon well-mixed periods. The prediction was made based on the California-specific emission maps.

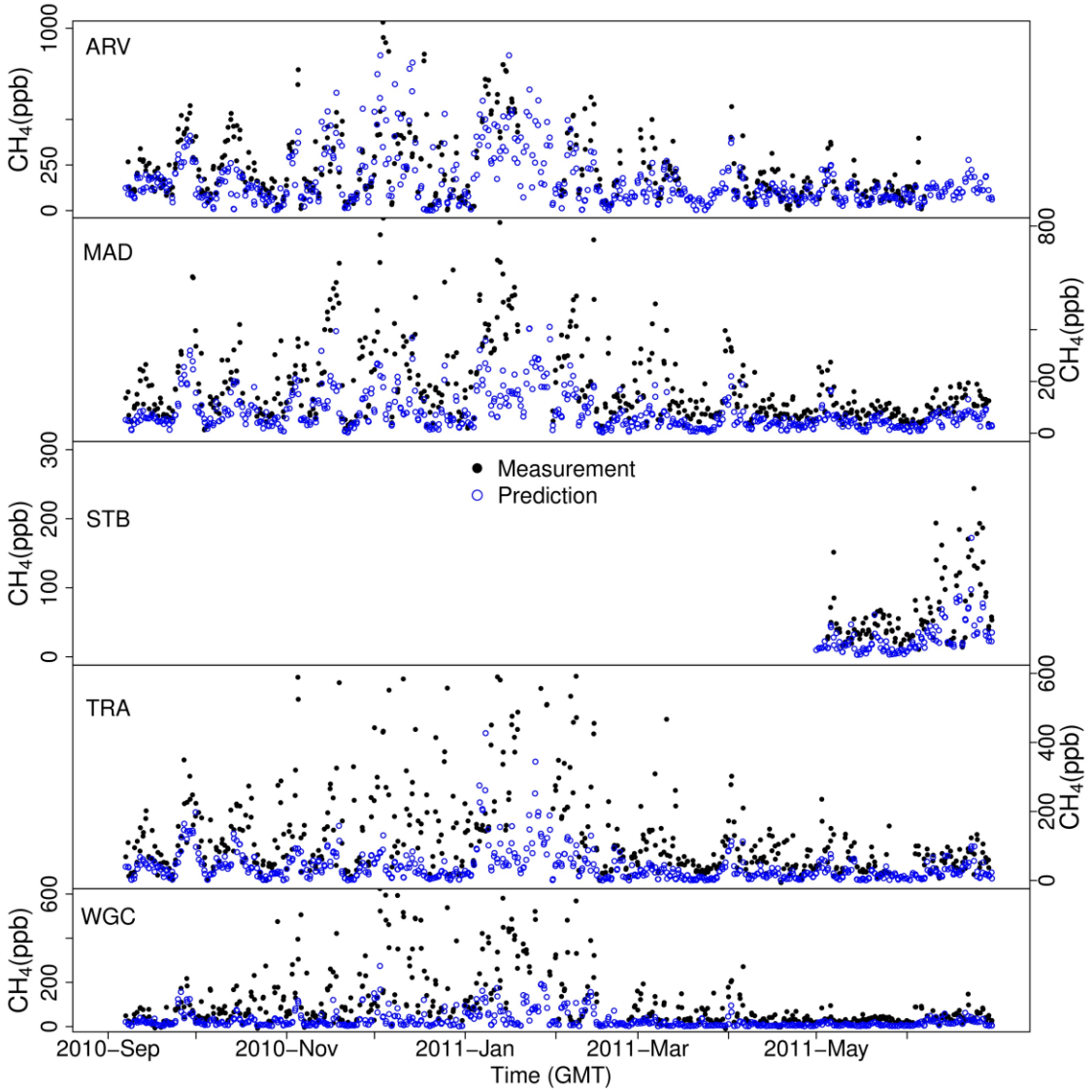

Figure 11. Time series of measured and predicted mixing ratios at the five network sites during noon-afternoon well-mixed periods.

3.2. Footprints

Figure 12 shows the average CH_4 footprints for May – June 2011 and compares the average footprints between the cases using one site and multiple sites. When footprints for all five sites are combined, the sensitivity of surface emissions to the measurement sites are significantly improved, as compared to the results with one station only. The combined footprints from multiple sites extend the sensitivity over most of the Central Valley. Figure 13 shows average footprints for other seasons. There is a clear seasonal pattern for the distribution of footprints, which is important to attribute signals to different emission sources for each season. Overall, the seasonal footprints are strong in the north-south direction in the Central Valley although footprints are strong in the west-east direction near the WGC site for some seasons. For example,

summer footprints are strongest from the San Francisco Bay Area to the west of the WGC tower due to the dominance of land-ocean winds. Also, there is a shift of footprints toward north-south winds from west-east winds during the transition seasons of spring and fall, which is a similar result to that described in Jeong et al. [2012a] and Jeong et al. [2012b]. Depending on the season, the footprints reach the Southern California Air Basin (i.e., Region 10), which allows for constraining important urban emissions.

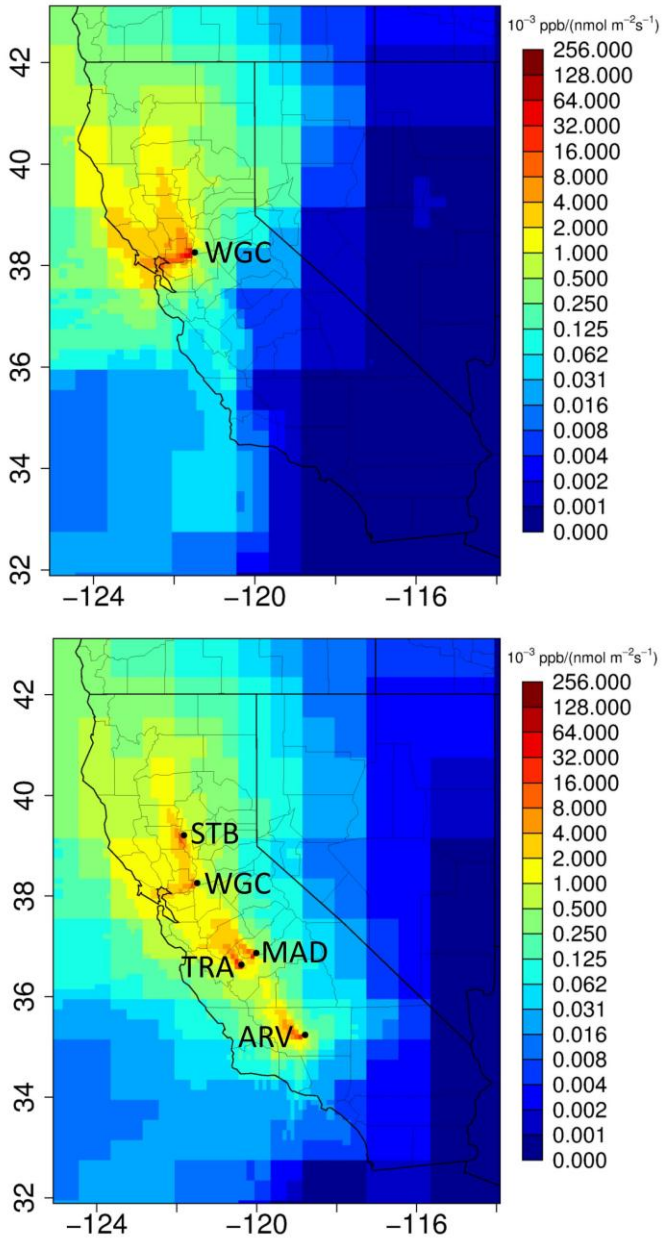

Figure 12. Averaged footprints during the noon-afternoon hours for (a) the WGC site and (b) all five sites during May – June 2011.

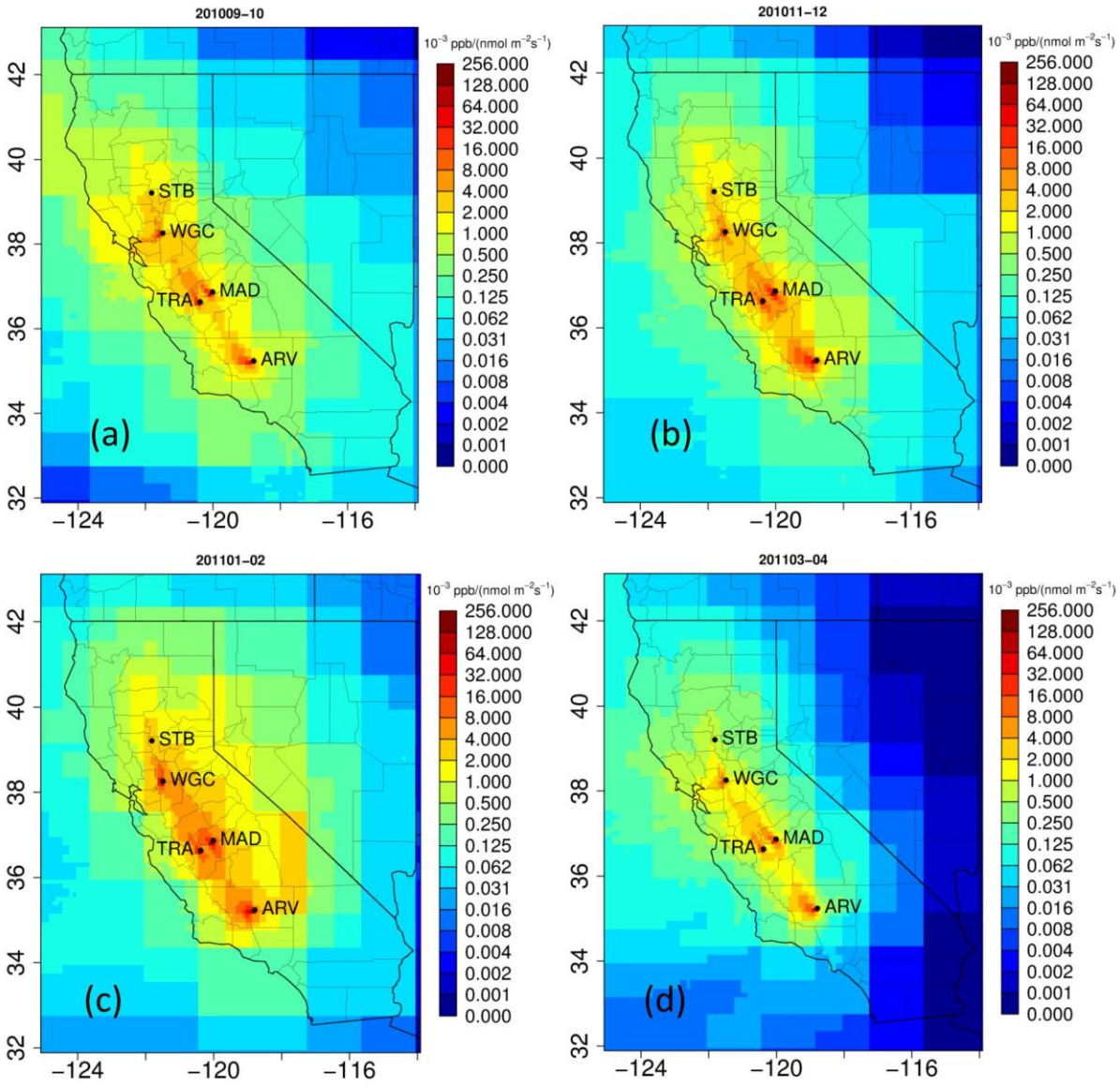

Figure 13. Seasonal mean footprints during the noon-afternoon hours for (a) September – October 2010, (b) November – December 2010, (c) January – February 2011 and (d) March – April 2011.

3.3. Bayesian Inverse Analysis

3.3.1. Linear Analysis

Bayesian inverse analysis was conducted using two different emission models: California-specific emission model and EDGAR42. For each emission model, we performed inversion for both region and source analyses. For region analysis, we estimated CH_4 emissions from the different regions in Figure 5d using a scaling factor Bayesian inversion (SFBI) method. The

source analysis optimizes scaling factors for each emission source. Figure 14 shows the comparison result between measured CH_4 signals and those predicted based on the California specific emission model using a chi-squared (fitexy) linear regression analysis [Press et al., 1992] during May 2011 before and after inverse optimization. In the figure, outliers are removed after initial inversion [Bergamaschi et al., 2005].

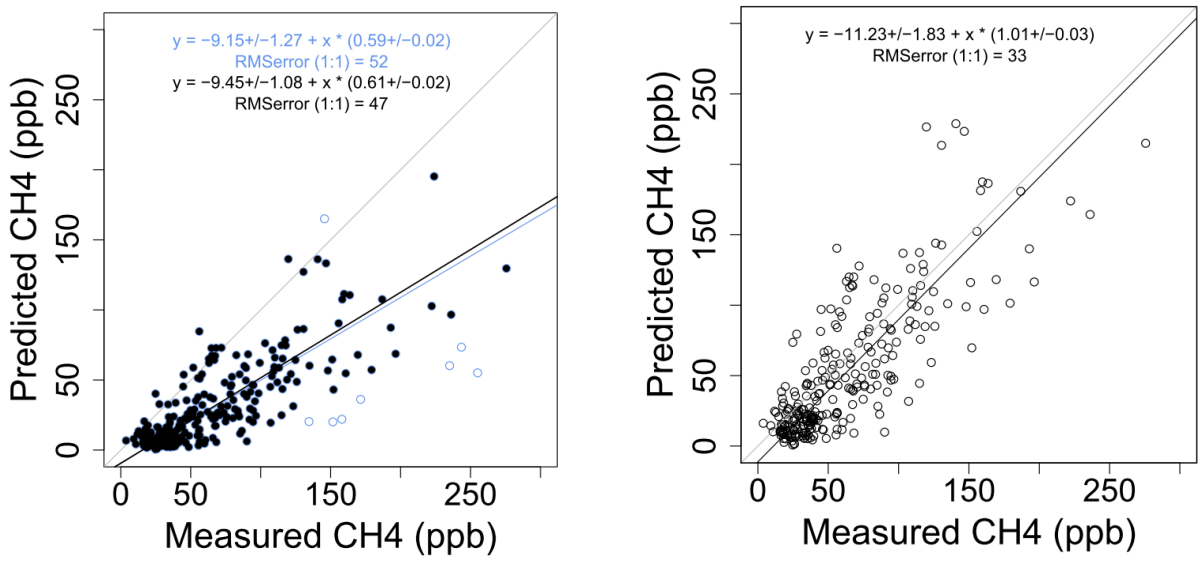

Figure 14. Comparison of California-specific predicted vs. measured CH_4 signals during May 2011 before (left) and after (right) inverse optimization. The light blue circles indicate those removed after the first inversion.

Table 4 summarizes the linear analysis results before and after Bayesian region inversion where emissions for each sub-region are scaled based on the optimized scaling factors for 14 sub-regions including the region outside California. Depending on the month, predicted CH_4 signals using the California-specific emission model are typically 40 – 80% of measurements before inversion, while EDGAR42 prior signals are only 20 – 40% of measurements before inverse optimization. After inversion with the 50% error assumption in the prior emissions, the posterior CH_4 signals based on the California-specific emission model are consistent with the measurements for most of the months, while the posterior signals from EDGAR42 are still systematically lower than the measurements. This suggests that EDGAR42 in the Central Valley are systematically too low where footprints are strong.

Table 4. Linear Analysis Results Before and After Bayesian Region Inversion

		Sep	Oct	Nov	Dec	Jan	Feb	Mar	Apr	May	June
						Before Inversion					
CA[a]	Slope	0.79±0.03	0.63±0.05	0.74±0.05	0.78±0.07	0.70±0.08	0.4±0.03	0.56±0.03	0.69±0.02	0.59±0.02	0.46±0.04
	RMS[c]	50	97	137	214	281	138	97	66	52	63
ED42[b]	Slope	0.28±0.02	0.30±0.04	0.27±0.01	0.23±0.02	0.23±0.02	0.25±0.03	0.23±0.01	0.28±0.01	0.28±0.01	0.36±0.05
	RMS	90	113	171	249	334	156	119	90	68	69
						After Inversion					
CA	Slope	1.00±0.04	0.95±0.05	0.91±0.05	0.94±0.07	1.01±0.10	0.80±0.06	0.99±0.04	1.03±0.03	1.01±0.03	0.96±0.04
	RMS	38	57	108	148	227	104	72	49	33	33
ED42	Slope	0.64±0.03	0.74±0.04	0.79±0.03	0.77±0.05	0.65±0.05	0.55±0.04	0.64±0.03	0.81±0.02	0.86±0.03	0.87±0.05
	RMS	55	51	92	134	230	106	79	49	34	34

[a]California-specific emission model
[b]EDGAR42 emission model
[c]Units of ppb

3.3.2. Bayesian Region Analysis

The Bayesian region analysis estimates scaling factors for sub-regions using the Bayesian inverse technique (see Figure 5d for sub-region classification). In this study, a total of 14 scaling factors including the region outside California are solved for a given inversion period. Although the inversions are performed at the monthly temporal scale, inferred CH_4 emissions are reported by season and as a regional sum over the regions where the total emissions are significant and footprints show sensitivity. Since our data do not cover a full year, we divided the 10 months into five seasons instead of four seasons.

Figure 15 shows the posterior emission estimates using the California-specific emission model by region and season. Overall, the inversion results suggest that actual CH_4 emissions are higher than the prior emissions for most of the regions and seasons. In particular, the posterior emissions are significantly higher than the prior in Regions 6, 8, and 12 where the emissions are well constrained. For Region 10 (Southern California region), the posterior uncertainties are reduced for some seasons, suggesting that the measurements in the Central Valley weakly constrain the emissions in Region 10. In Region 7 (Bay Area and surrounding urban area), summer emissions are slightly higher than the other seasons. The significantly higher emissions in Region 8 suggest that emissions from dairy sources are significantly higher than the prior. Also, the high emissions in Region 12 are likely related to the dairy emissions (~80% of region total). The results in Figure 15 also show that there is a clear seasonal variation in CH_4 emissions. For example, in Region 6 where high emissions are expected from rice agriculture, the posterior emissions are high during the fall (i.e., fall 2010) and later spring-early summer season.

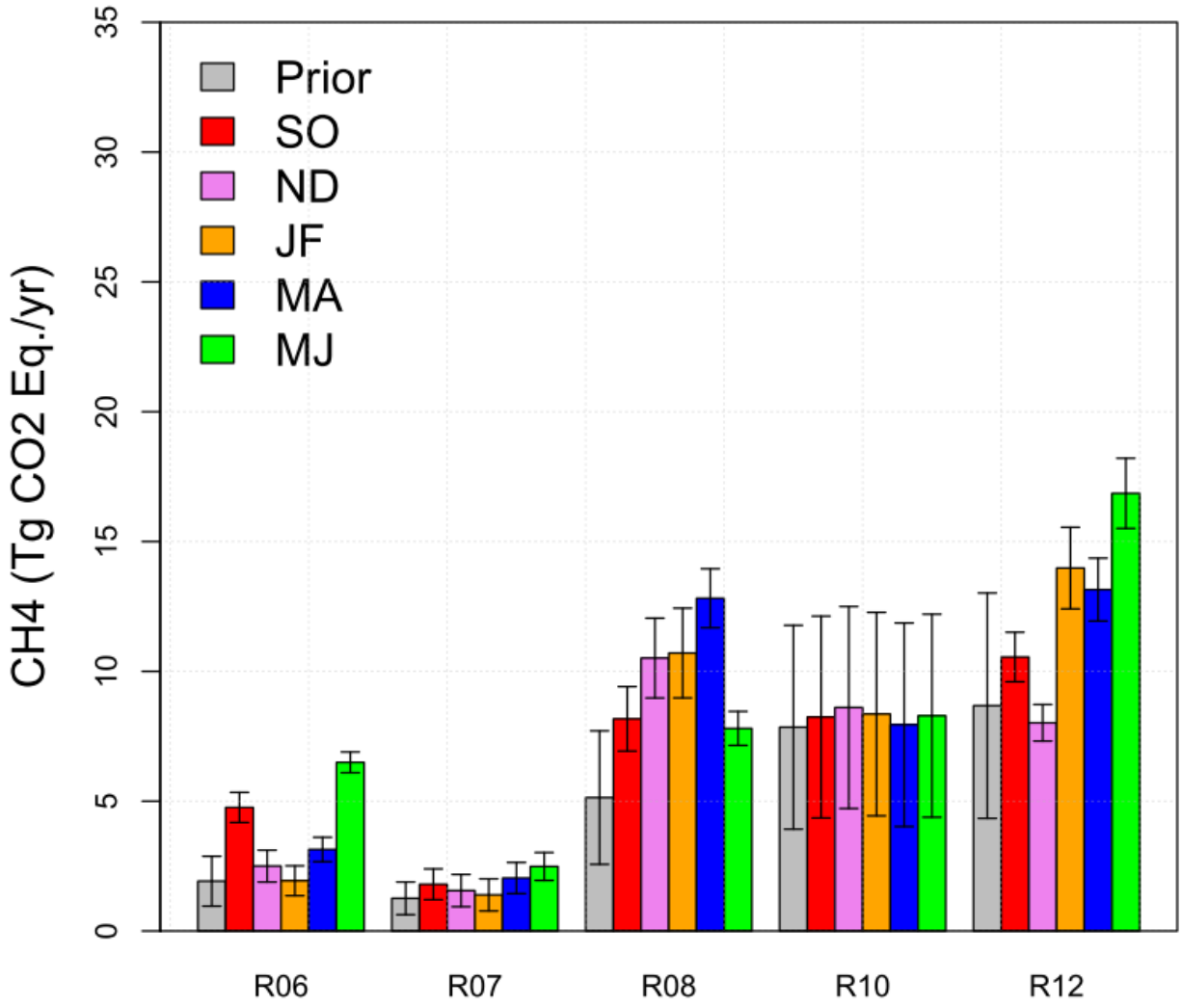

Figure 15. Estimates of posterior CH_4 emissions (Tg CO_2eq yr^{-1}) by region and season based on the California-specific emission model. Only regions with significant emissions are shown. The annual mean prior (gray bar) represents the annual average of seasonally varying emissions and is compared with posterior seasonal emissions (color bars).

Figure 16 shows the region analysis results using the EDGAR42 emission model. The inversion results based on EDGAR42 show different emission estimates, yielding generally higher emissions for most of the regions compared to those of the California-specific case. In Region 12, for instance, the EDGAR42-based inverse modeling estimates consistently higher CH_4 emissions than those from the California-specific modeling, although the EDGAR42 prior emission is lower than that of the California-specific model. As shown in Figure 16, the annual average scaling factor for Region 12 is ~3, which yields 15.2±1.6 Tg CO_2eq yr^{-1}.

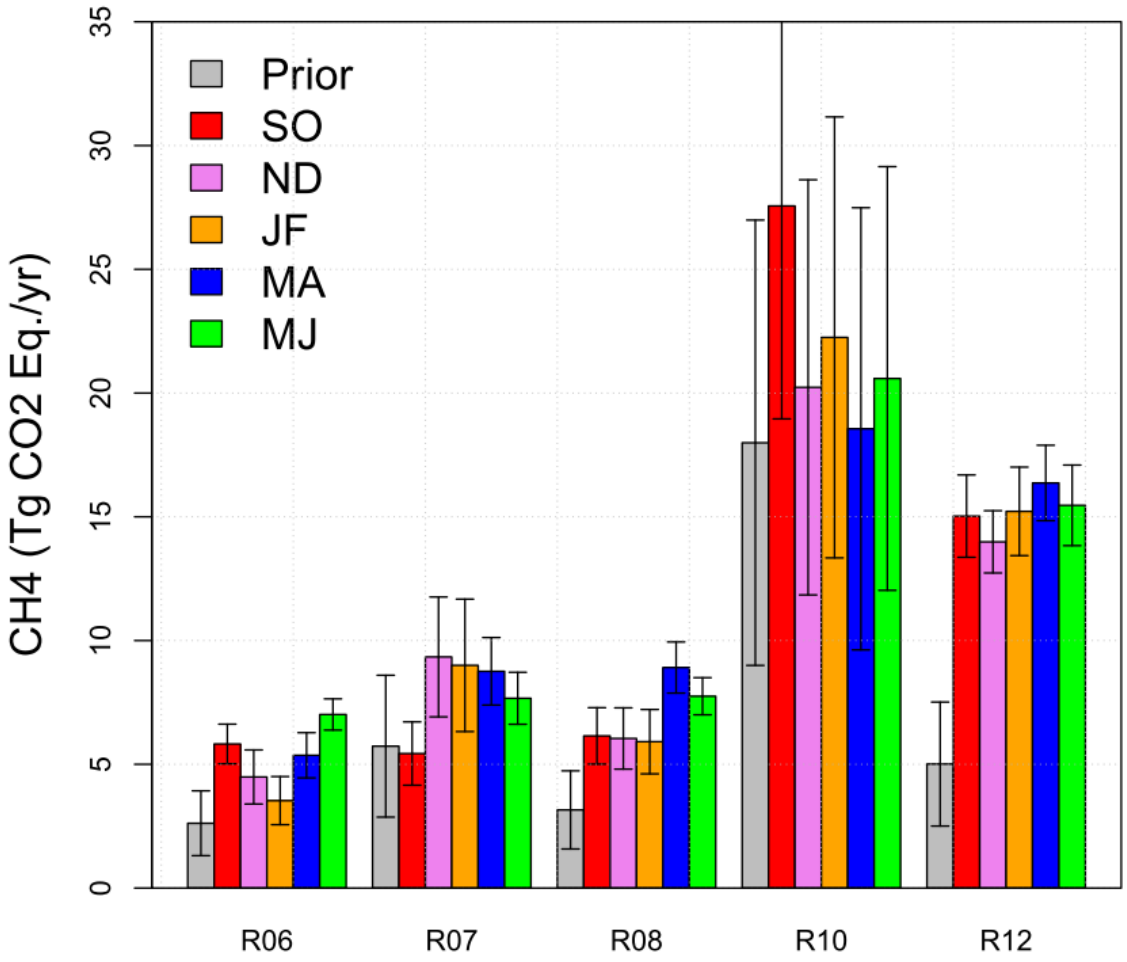

Figure 16. Estimates of posterior CH_4 emissions (Tg CO_2eq yr^{-1}) by region and season based on the EDGAR42 emission model. Only regions with significant emissions are shown.

Results of the region analysis show that the sum of the posterior emissions for the sub-regions in the Central Valley (i.e., Regions 6, 8 and 12) are similar for the California specific and EDGAR42 *a priori* emission models (see Table 5). The current measurement network constrains annual average CH_4 emissions for Regions 6, 8 and 12 to be between 26.3±1.8 and 27.4±2.1 for the California-specific and EDGAR42 emission models respectively, assuming uncorrelated errors between regions. However, there are significant differences in the predominantly urban regions (7 and 10) where the EDGAR42 model shows higher CH_4 emissions than those estimated with the California-specific model by a factor of ~3. This is because the prior emissions show the same pattern, with EDGAR42 higher than California-specific by a factor of 2.6 (23.7 vs. 9.1 Tg CO_2eq yr^{-1}). This result is consistent with that reported in Jeong et al. [2012a] where the estimated annual emission for Region 7 using EDGAR32 (version 3.2) is higher than that estimated with the California-specific model by a factor of ~4. Although the results using multiple emission models help to characterize the uncertainty associated with estimating emissions at the sub-regional scale, this result demonstrates that additional

measurements are required in the San Francisco Bay and Southern California areas in order to strongly constrain emissions from those urban regions.

Table 5. Comparison of Annual CH_4 Emission (Tg CO_2eq) between the EDGAR42 and California-specific Emission Models

Emission Model	Region	R01	R02	R03	R04	R05	R06	R07	R08	R09	R10	R11	R12	R13	Total
CA-specific	Emissions	0.2	0.3	0.4	0.4	0.7	3.8	1.9	10.0	1.0	8.3	0.2	12.5	0.2	39.8
	Uncertainty[a]	0.1	0.1	0.2	0.2	0.3	0.5	0.6	1.3	0.5	3.9	0.1	1.2	0.1	4.4
EDGAR	Emissions	0.1	0.4	0.7	0.4	0.5	5.2	8.0	7.0	1.2	21.8	0.3	15.2	0.5	61.4
	Uncertainty	0.0	0.2	0.3	0.2	0.2	0.9	1.8	1.1	0.6	8.7	0.2	1.6	0.2	9.1

[a]Posterior uncertainty = 1σ

Using the posterior results from the California specific region analysis we evaluate the total and source sector emissions for the sub-regions of the Central Valley where the measurements have most weight. We justify the use of the California-specific model, rather than EDGAR42 emission model, because the linear analysis results (Table 4) showed that the posterior signals based on the California-specific model are in much better agreement with the measurements than those of EDGAR42. Table 6 shows the annually averaged CH_4 emissions for Regions 6, 8 and 12, which account for 56% of the total emission in the California-specific *a priori* model. The emission for each sector within a given region was calculated by multiplying the *a priori* sector emissions with the optimized scaling factor for the region. We observe that emissions from Region 6 are composed of a mixture of rice agriculture, livestock, natural gas, and wetlands, while Region 8 and 12 are dominated by livestock emissions.

Table 6. Estimated Annual CH_4 Emissions (Tg CO_2eq) for Regions 6, 8, and 12 by Sector Based on the California-specific Emission Model

Sector	Region 6		Region 8		Region 12	
	Prior	Posterior	Prior	Posterior	Prior	Posterior
CP	0.50	0.98±0.14	0.01	0.02±0.00	0.00	0.00±0.00
LF	0.31	0.60±0.08	0.33	0.65±0.08	0.95	1.37±0.13
DLS	0.36	0.71±0.10	3.79	7.37±0.93	5.77	8.32±0.77
NDLS	0.19	0.37±0.05	0.54	1.05±0.13	1.00	1.44±0.13
NG	0.33	0.65±0.09	0.10	0.19±0.02	0.11	0.16±0.02
PL	0.03	0.06±0.01	0.02	0.03±0.00	0.71	1.03±0.10
WW	0.03	0.06±0.01	0.08	0.16±0.02	0.11	0.16±0.01
WL	0.18	0.35±0.05	0.27	0.52±0.07	0.02	0.03±0.00
Total	1.92	3.77±0.53	5.14	9.99±1.26	8.68	12.52±1.16

3.3.3. Bayesian Source Analysis

We also used the Bayesian inverse analysis to estimate the emissions by inferring state-wide scaling factors for each emission source instead of each sub-region. The results show that while posterior emissions from livestock are similar for the California specific and EDGAR42 models,

emissions from landfill (solid waste) and natural gas production and use are both substantially higher when using the EDGAR42 prior. Figure 17 shows the source analysis results using the California-specific emission model. These results are consistent with those of the counterpart inverse analysis for regional emissions. For example, the source inversion suggests that actual emissions from livestock are much higher than the prior. This result agrees with the higher posterior emissions in Region 8 where livestock emissions are dominant (~80% of annual CH_4 emissions). Also, the results indicate that the posterior emissions for crop agriculture are higher during fall and summer season than the prior, which are consistent with the higher emissions in Region 6, where high biogenic emissions are expected from rice agriculture. While Figure 17 shows that CH_4 emissions from natural gas sources are generally higher than the prior, more measurements are required to effectively constrain natural gas emissions from the large urban areas including the Southern California region.

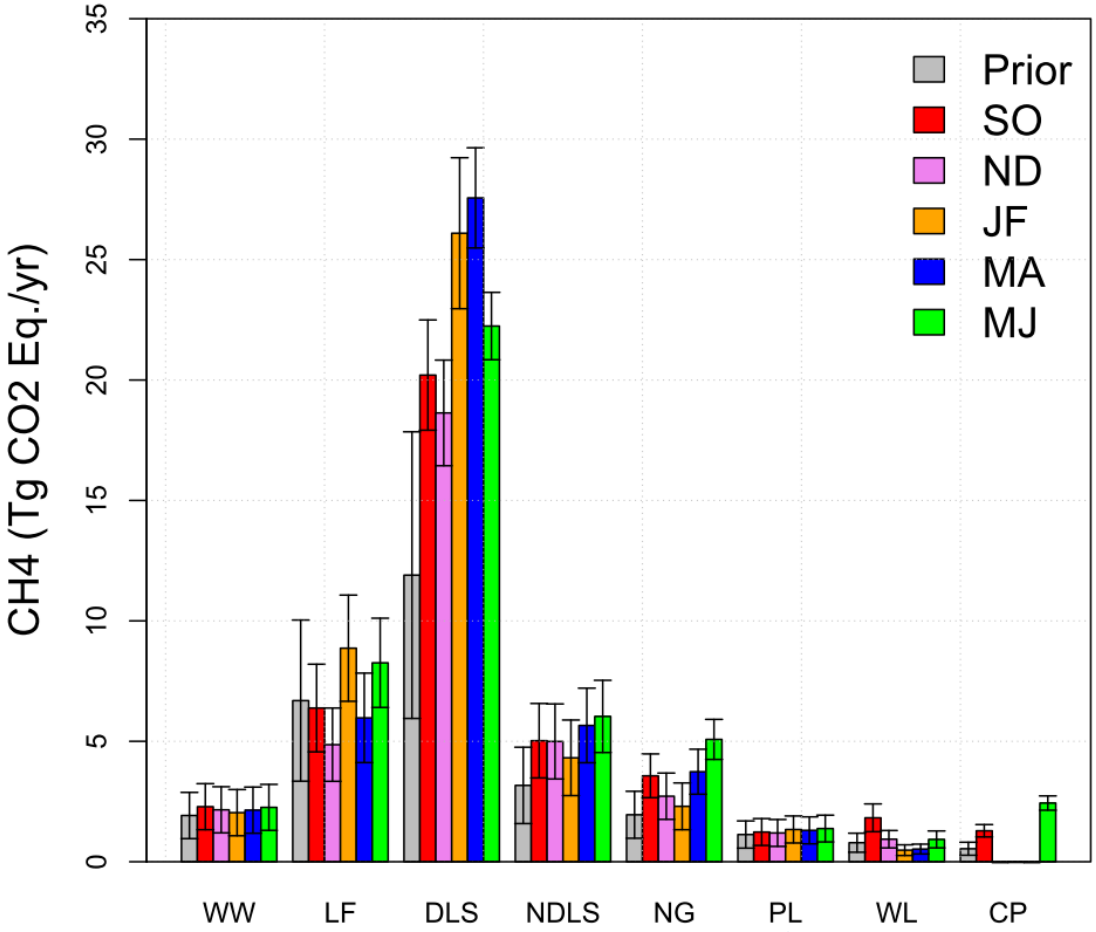

Figure 17. Estimates of posterior CH_4 emissions (Tg CO_2eq yr^{-1}) for California by source and season based on the California-specific emission model. WW, LF, DLS, NDLS, NG, PL, WL and CP represent wastewater, landfill, dairy livestock, non-dairy livestock, natural gas, petroleum, wetland, and crop agriculture sources, respectively.

The source analysis results based on EDGAR42 are shown in Figure 18, where eight major sources (~95% of total emissions) out of a total of 16 sources are compared. As one might expect from the region analysis result, the source analysis based on EDGAR42 shows

significantly different posterior emissions for some of the sources, compared to the California-specific case. In particular, the annual CH_4 emission estimate for solid waste (equivalent to landfill of the California-specific model) from EDGAR42 is 24.0±5.1 Tg CO_2eq, which is significantly higher than that (6.9±1.9) estimated using the California-specific model.

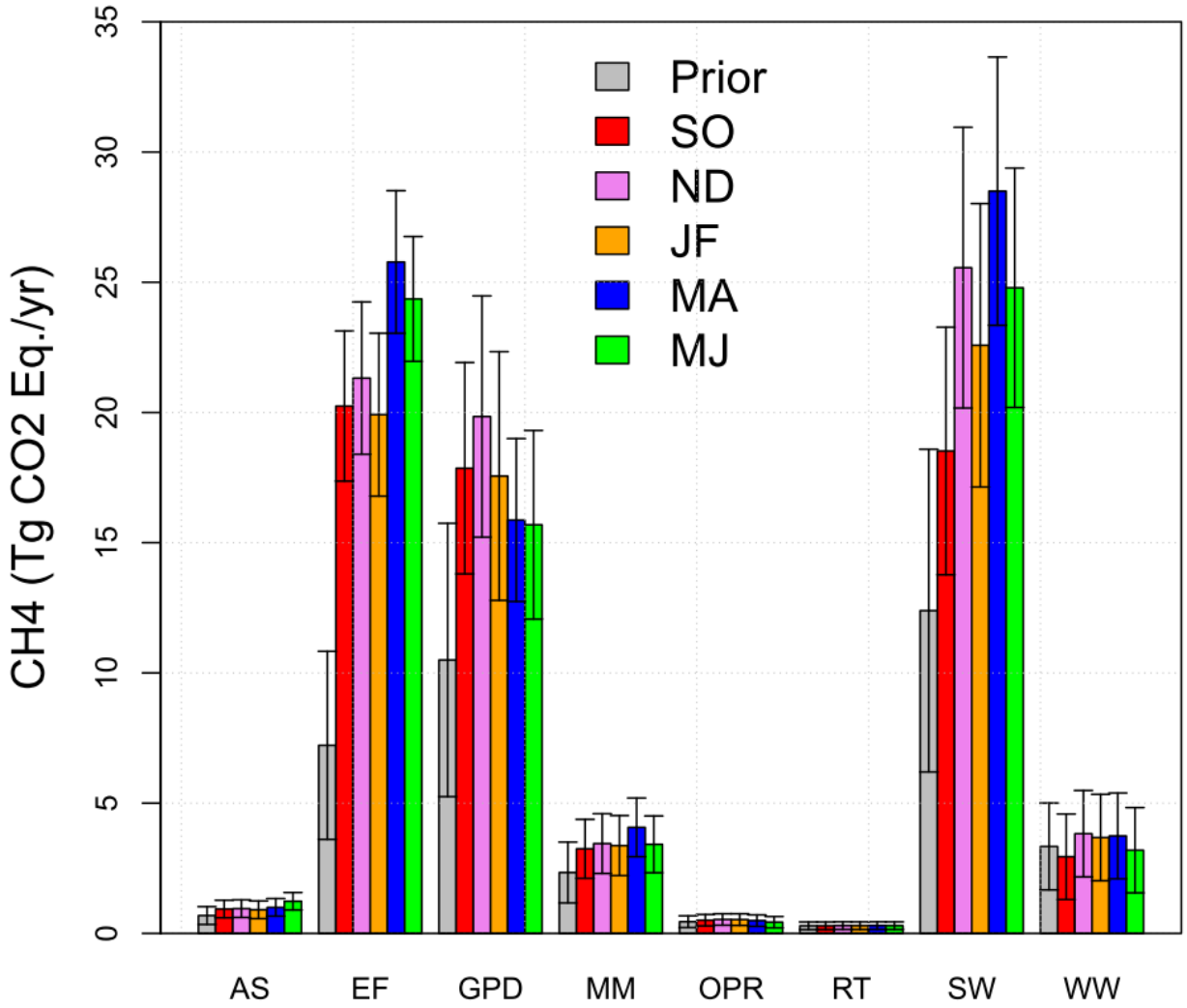

Figure 18. Estimates of posterior CH_4 emissions (Tg CO_2eq yr^{-1}) for California by source and season based on the EDGAR42 emission model. AS, EF, GPD, MM, OPR, RT, SW, and WW represent agricultural soils, enteric fermentation, gas production and distribution, manure management, oil production and refineries, road transportation, solid waste, and wastewater, respectively.

Table 7 summarizes the estimated annual CH_4 emissions using the two independent CH_4 emission models. Overall, the EDGAR42-based emission estimates are higher than those of the California-specific model. Also, the source-based inversion analysis estimates slightly higher emissions compared to those of the region analysis. The Bayesian region analysis suggests that the total posterior CH_4 emission for the entire California is 1.2±0.1 times and 1.9±0.3 times higher than the current CARB inventory (32 Tg CO_2eq; CARB, 2011) based on the inverse modeling results using the California-specific and EDGAR42 emission models, respectively. The

source analysis suggests slightly higher emissions, which are 1.4±0.1 times and 2.3±0.2 times the current CARB inventory for the California-specific model and the EDGAR42 model, respectively. Note that we do not include the emissions estimated from the source analysis using EDGAR42 in the executive summary because of the significant uncertainty associated with the large urban areas.

Our State total CH_4 emission estimates from different inverse analyses are compared with an estimate based on Wennberg et al. [2012] where the urban emissions in the Southern California region are better constrained. For California's South Coast Air Basin (the larger Los Angeles metropolitan region, hereafter LA region), Wennberg et al. [2012] estimated a total CH_4 emission of 0.44±0.15 Tg yr^{-1}, which is 1.4 – 2.8 times higher than the California-specific prior emission and 0.4 – 0.9 times EDGAR42 for the LA region. This suggests that scaling EDGAR42 emissions by a factor of much greater than 1 based on the inversion results for the Central Valley will substantially overestimate State total CH_4 emissions. A more reasonable approach for State total emissions can be estimated by using the posterior emissions from the California-specific model for the Central Valley and other non-urban regions and scaling the California-specific prior emissions for the large urban regions (7 and 10) by a factor of 1.4 - 2.8. This approach estimates total CH_4 emissions of 42 - 55 Tg CO_2eq yr^{-1}, where the uncertainty is dominated by the urban regions. This estimate for State total CH_4 emissions is consistent with the results of our inverse analyses (Table 7) except for the EDGAR42 source analysis.

Table 7. Summary of Estimated Annual CH_4 Emissions (Tg CO_2eq; GWP = 21) for California

Emission Model	Region Analysis	Source Analysis
California-specific	39.8±4.4	43.6±3.6
EDGAR42	61.4±9.4	73.7±7.4

4. Conclusions and Recommendations

- The current GHG network constrains annual average CH_4 emissions from California's Central Valley to be between 26.3±1.8 Tg CO_2eq and 27.4±2.1 Tg CO_2eq for the California-specific and EDGAR42 emission models respectively. Similarly, emissions from livestock (which are predominantly located in the Central Valley) are estimated to be 28.2±3.4 Tg CO_2eq and 25.8±3.2 Tg CO_2eq from the California-specific and EDGAR42 emission models, respectively.

- While significant error reductions are obtained in California's Central Valley, emissions from other regions remain uncertain, with the ratio of emissions to the current California CH_4 emission inventory (32 Tg CO_2eq yr^{-1}) ranging from 1.2±0.1 and 1.9±0.3 from the Bayesian region analysis based on the California-specific and EDGAR42 emission

models. Hence, additional tower measurements in the San Francisco Bay and Southern California areas are required to constrain those emissions.

- Noting the large uncertainty in urban emissions estimated from measurements in the Central Valley, emissions from large urban areas (San Francisco Bay Area and Southern California region) are estimated based on a recent study in the larger Los Angeles metropolitan region to better constrain large urban emissions. Combined with the emissions from the Central Valley and other non-urban regions, State total CH_4 emissions are estimated to be 1.3 – 1.7 times larger than the current State total CH_4 emissions where the uncertainty is dominated by uncertainty in the urban regions. This further suggests that additional measurements in the San Francisco Bay and Southern California areas are required to constrain those emissions.

- Data from the current CH_4 measurement network are effective for use in constraining emissions from different regions of California's Central Valley but cannot be used to uniquely attribute emissions to specific source sectors. Additional measurements of source specific tracers (e.g., CO, VOCs, and potentially $_CH_4$ isotopes) will help separate different sources of CH_4.

- Currently, uncertainty in the inverse model estimates of CH_4 emissions for regions containing measurement sites are dominated by uncer$_t$ainty in the meteorological modeling of trace gas transport (e.g., winter) and estimation of background signals (e.g., summer). Additional work is needed to identify the source of these errors and reduce them.

5. References

Bergamaschi, P., M. Krol, F. Dentener, A. Vermeulen, F. Meinhardt, R. Graul, M. Ramonet, W. Peters, and E. J. Dlugokencky (2005), Inverse modelling of national and European CH_4 emissions using the atmospheric zoom model TM5. Atmos. Chem. Phys., 5, 2431–2460.

CARB (2010), California Greenhouse Gas Emissions Inventory. California Air Resources Board Staff Report. (http://www.arb.ca.gov/cc/inventory/inventory.htm)

CARB (2011), California Greenhouse Gas Emissions Inventory. California Air Resources Board Staff Report. (http://www.arb.ca.gov/cc/inventory/inventory.htm)

Dye, T.S., C. G. Lindsey, and J. A. Anderson (1995), Estimates of mixing depth from "boundary layer" radar profilers. Preprints from the 9th Symposium on Meteorological Observations and Instrumentation, Charlotte, NC, March 27-31, 156-160 (STI-94212-1451).

EDGAR42 database: Emission Database for Global Atmospheric Research (EDGAR), release version 4.2, http://edgar.jrc.ec. europa.eu, European Commission, Joint Research Centre (JRC)/Netherlands Environmental Assessment Agency (PBL), 2012.

Gerbig, C, J. Lin, S. Wofsy, B. Daube, A. E. Andrews, B. Stephens, P. S. Bakwin and C. Grainger (2003), Toward constraining regional-scale fluxes of CO_2 with atmospheric observations over a continent: 2. Analysis of COBRA data using a receptor-oriented framework. J. Geophys. Res., 108(D24), doi:10.1029/2003JD003770.

Gimson, N. R. and Uliasz, M. (2003), The determination of agricultural methane emissions in New Zealand using receptor-oriented modeling techniques. Atmos. Environ., 37, 3903-3912.

Göckede, M., A. M. Michalak, D. Vickers, D. P. Turner, and B. E. Law (2010), Atmospheric inverse modeling to constrain regional-scale CO_2 budgets at high spatial and temporal resolution. J. Geophys. Res., 115, D15113, doi:10.1029/2009JD012257.

Hofman, D. J., J. H. Butler, E. J. Dlugokencky, J. W. Elkins, K. Masarie, S. A. Montzka, and P. Tans (2006), The role of carbon dioxide in climate forcing from 1979 - 2004: Introduction of the Annual Greenhouse Gas Index. Tellus B, 58B, 614-619.

Houweling, S., T. Kaminski, F. Dentener, J. Lelieveld, and M. Heimann (1999), Inverse modeling of methane sources and sinks using the adjoint of a global transport model. J. Geophys. Res., 104(D21), 26137-26160.

IPCC (1995), IPCC Second Assessment Report (SAR), "Climate Change 1995".

Janjic, Z. I. (1990), The step-mountain coordinate: physical package. Mon. Weather Rev., 118, 1429–1443.

Jeong, S., C. Zhao, A. E. Andrews, L. Bianco, J. M. Wilczak, and M. L. Fischer (2012a), Seasonal variation of CH4 emissions from central California. J. Geophys. Res., 117, D11306, doi:10.1029/2011JD016896.

Jeong, S., C. Zhao, A. E. Andrews, E. J. Dlugokencky, C. Sweeney, L. Bianco, J. M. Wilczak, and M. L. Fischer (2012b), Seasonal variations in N_2O emissions from central California. Geophys. Res. Lett., 39, L16805, doi:10.1029/2012GL052307.

Kort, E. A., J. Eluszkiewicz, B. B. Stephens, J. B. Miller, C. Gerbig, T. Nehrkorn, B. C. Daube, J. O. Kaplan, S. Houweling, and S. C. Wofsy (2008), Emissions of CH_4 and N_2O over the United States and Canada based on a receptor-oriented modeling framework and COBRA-NA atmospheric observations. Geophy. Res. Lett., 35, L18808, doi:10.1029/2008GL034031.

Lin, J. C., C. Gerbig, S. C. Wofsy, A. E. Andrews, B. C. Daube, C. A. Brainger, B. B. Stephens, P. S. Bakwin, and D. Y. Hollinger (2004), Measuring fluxes of trace gases at regional scales by Lagrangian observations: Application to the CO_2 Budget and Rectification Airborne (COBRA) study. J. Geophys. Res., 109, D15304, doi:10.1029/2004JD004754.

Lin, J. C., C. Gerbig, S. C. Wofsy, A. E. Andrews, B. C. Daube, K. J. Davis, and C. A. Grainger (2003), A near-field tool for simulating the upstream influence of atmospheric observations: The Stochastic Time-Inverted Lagrangian Transport (STILT) model. J. Geophys. Res., 108(D16), 4493, doi:10.1029/2002JD003161.

Mellor G. L. and T. Yamada (1982), Development of a turbulence closure model for geophysical fluid problems. Rev. Geophys. Space Phys. 20, 851–875.

Mesinger, F., G. DiMego, E. Kalnay, K. Mitchell, P. C. Shafran, W. Ebisuzaki, D. Jovic, J. Woollen, E. Rogers, E. H. Berbery, M. B. Ek, Y. Fan, R. Grumbine, W. Higgins, H. Li, Y. Lin, G. Manikin, D. Parrish, and W. Shi (2006), North American Regional Reanalysis. Bull. Amer. Meteor. Soc., 87 (3), 343-360.

Miller, S. M., D. M. Matross, A. E. Andrews, D. B. Millet, M. Longo, E. W. Gottlieb, A. I. Hirsch, C. Gerbig, J. C. Lin, B. C. Daube, R. C. Hudman, P. L. S. Dias, V. Y. Chow, and S. C. Wofsy (2008), Sources of carbon monoxide and formaldehyde in North America determined from high-resolution atmospheric data. Atmos. Chem. Phys., 8, 7673-7696.

Montzka, S. A., E. J. Dlugokencky1, and J. H. Butler (2011) Non-CO_2 greenhouse gases and climate change. Nature, 476, 43-50.

Nehrkorn, T., J. Eluszkiewicz, S. C. Wofsy, J. C. Lin, C. Gerbig, M. Longo, and S. Freitas (2010), Coupled weather research and forecasting - stochastic time-inverted lagrangian transport (WRF-STILT) model. Meteor. Atmos. Phys., 107 (1), 51-64, doi:10.1007/s00703-010-0068-x.

Potter, C., S. Klooster, S. Hiatt, M. Fladeland, V. Genovese and P. Gross (2006), Methane Emissions from Natural Wetlands in the United States: Satellite-Derived Estimation Based on Ecosystem Carbon Cycling. Earth Interactions, 10, 1–12.

Press, W. H., S. A.Teukolsky, W. T. Vetterling, and B.P. Flannery (1992), Numerical Recipes, 2nd edition. Cambridge: Cambridge University Press.

Salas, W., P. Green, S. Frolking, C. Li and S. Boles (2006), Estimating Irrigation Water Use for California Agriculture: 1950s to Present. California Energy Commission, PIER Energy-Related Environmental Research. CEC-500-2006-057.

Skamarock, W.C., J. B. Klemp, J. Dudhia, D.O. Gill, D. M. Barker, X. Z. Huang, W. Wang, and J. G. Powers (2008), A description of the advanced research WRF version 3. Technical Note 475+STR. Mesoscale and Microscale Meteorology Division, NCAR, Boulder, Colorado.

Wennberg, P. O., W. Mui, D Wunch, E. A. Kort, D. R. Blake, E. L. Atlas, G. W. Santoni, S. C. Wofsy, G. S. Diskin, S. Jeong, and M. L. Fischer (2012), On the Sources of Methane to the Los Angeles Atmosphere. Environ. Sci. Technol., 46 (17), 9282 - 9289, doi:10.1021/es301138y.

Zhao, C., A. E. Andrews, L. Bianco, J. Eluszkiewicz, A. Hirsch, C. MacDonald, T. Nehrkorn, and M. L. Fischer (2009), Atmospheric inverse estimates of methane emissions from Central California. J. Geophys. Res., 114, D16302, doi:10.1029/2008JD011671.